Metal Nanoparticle Deposition On Biological And Physical Scaffolds To Develop A New Class Of Electronic Devices

Vikas Berry

Dissertation submitted to the faculty of the
Virginia Polytechnic Institute and State University
in partial fulfillment of the requirements for the degree of

Doctor of Philosophy
In

Chemical Engineering

David F Cox, Chair
Ravi F Saraf
Donald G Baird
Richey M Davis

September 5, 2006
Blacksburg, Virginia

Keywords: Nanotechnology, Bio-MEMS, Electron Tunneling, Bacteria

Metal Nanoparticle Deposition On Biological And Physical Scaffolds To Develop A New Class Of Electronic Devices

Vikas Berry

(ABSTRACT)

Nanoparticle based devices are becoming of great interest because of their single-electron transport behavior, and high surface charge density. Nanoparticle based devices operate at low power, and are potentially highly stable and extremely robust. Making interconnections to nanoparticle devices, however, has been an impending issue. Also percolating/conductive array of nanoparticles is not easy to build since repulsion between the charged nanoparticles causes them to deposit at distance significantly larger for electron tunneling. In this study, we resolve these challenges to make nanoparticle based electronic devices. Using biological (bacteria) or physical (polyelectrolyte fiber) scaffolds, we selectively deposited percolating array of 30 nm Au nanoparticles, to produce a highly versatile nanoparticle-organic hybrid device. The device is based on electron tunneling phenomena, which is highly sensitive to change in inter-particle distance and dielectric constant between nanoparticles. The key to building this structure is the molecular brushes on the surface of the scaffold, which shield the charge on nanoparticle to allow for percolating deposition. The electrostatic attraction for such a deposition on bacteria was measured to be so strong (0.038 N/m) that it could bend a 400

nm long and 25 nm wide gold nanorod. Once the device is built, the hygroscopic scaffolds were actuated by humidity, to modulate the electron tunneling barrier width (or height) between the metallic nanoparticles. A decrease in inter-particle separation by < 0.2 nm or a change in the dielectric constant from ~ 40 to 3 (for humidity excursion from 20% to ~0%), causes a 40-150 fold increase in electron tunneling current. The coupling between the underlying scaffold and the Au particle structure is essential to achieving such a high and robust change in current. In contrast to most humidity sensors, the sensitivity is extremely high at low humidity. This device is >10-fold better than standard microelectronic and MEMS technology based humidity sensors. After the deposition, the 'live' bacterial scaffold retains its biological construct, providing an avenue for active integration of biological functions with electronic transport in nanoparticle device. Such hybrids will be the key to conceptually new electronic devices that can be integrated with power and function of microorganisms, on flexible plastic-like substrates using simple beaker chemistry. The technology has broad potential based on variety of nanoparticles (for example, magnetic, metallic and semi-conducting) to make electro-optical and inorganic devices, bringing a prominent advancement in the present technology. Our work is published in, Angewandte Chemie, JACS and Nano Letters, and featured in places such as, Discover Magazine, Science News and Nature.

TABLE OF CONTENTS

LIST OF FIGURES

LIST OF TABLES

ACKNOWLEDGEMENT

This thesis is one of the best projects of my life so far. For this, my heartfelt gratitude goes to Dr. Ravi F. Saraf, my research advisor, for all his guidance and relentless support. I will always cherish those long discussions, sometime late in the night, that went on into this work. I have always been inspired by his words. I will always treasure his quotes. My favorite one – "*We cannot play God. We cannot create anything. We can only work with what Mother Nature provides*". It is a blessing to be under his tutelage. I want to thank him for his trust, vision and direction.

Also I would like to thank my PhD committee chair, Dr. David F. Cox and committee members Dr. Richey M. Davis and Dr. Donald G Baird for serving in my advisory committee and for their support. I also want to thank the faculty of Chemical Engineering for their support.

I thank Dr. Sendil Rangaswami, Dr. Subrata Kundu, and Dr. Rajinder Gill for their help in preparing bacterial cultures, nanoparticle solutions and nanofibers respectively. I want to thank Mike for his help in building chambers for vacuum measurements.

I want to thank my friends Gaurav Singh – my brother in arm, Vivek Maheshwari – Pranky Singh, Sanjun Niu, Jennifer Kane and Mohit – the Theekhi for making my stay memorable.

Last but not the least, I would like to thank my wife Namrita Vikas Berry, my mother Raj Berry and my father Col. V. K. Berry, for all their support and blessings.

1. OBJECTIVE

The ability of metal nanoparticles to allow electric current at single electron level[1], makes them the ultimate building block to fabricate nanodevices. These devices can work as single electron transistors and coulomb blockade devices. The problem however is inter-connecting such nanoparticles to power source. The small size of nanoparticles makes it difficult to connect them to macro-sized electrodes. One of the main objectives of this research is to build a system where the nanoparticles can be interconnected to a power source.

In such systems, the phenomena for electron transport between nanoparticles at different potentials is electron tunneling, which is highly sensitive to change in tunneling barrier width/height. For such devices, stimuli-assisted change in the barrier between nanoparticles would therefore sensitively change the conductivity of the device and thus will become a sensor of the stimuli. Another objective of this research is to achieve such stimuli-assisted change in electron tunneling barrier to produce change in electron tunneling conductivity.

This device will be based on simple self-assembly process. Recently self-assembly of nanoparticles on oppositely charge self-assembled polyelectrolyte surfaces has shown to produce electrically non-percolating arrays. Non-percolating deposition is a result of repulsion between similarly charged nanoparticles. An objective of this research is to show that nanoparticles deposited on polyelectrolyte “fingers” will shield the charge on the nanoparticle to produce percolating deposition.

Developments in nano- and bio- technology are showing potential to greatly impact the fabrication of future devices with high functionality and low-power. Also

nanostructure of microorganisms (such as virus[2,3], yeast[4]) and polyelectrolyte fibers, due to surface charge and biological affinities to specific molecules are attractive scaffolds to potentially template nanoparticles[2-7] for nanodevice applications. It is intended to show that bacterial cell surface having polyelectrolyte (Polyteichoic acid) fingers can be used to deposit nanoparticles having positive charge. The other objective of this research is to build polyelectrolyte fingers using polyelectrolyte fibers on silica and using that to deposit nanoparticles.

Using these simple nanoparticle arrays, it is intended to show that functional devices, based on changing the electron tunneling properties of the tunnel junction, could be built. Since the polyelectrolyte is hydrophilic in nature, the tunneling junctions is humidity sensitive, which will be used to build a humidity sensor.

2. INTRODUCTION

Nanoparticle films have been formed by processes such as spin coating[8], xerography[9], spraying[10], Langmuir-Blodgett deposition[11], electrostatic self-assembly[12,13], and covalent linkages using organic cross-linkers[14,15]. Recently, using the ionic nature of biomolecules such as proteins, DNA, and polysaccharides, some in-vivo and ex-vivo self-assemblies of metal, magnetic oxide, and semi-conducting nanoparticles have been fabricated[5,16-18]. In-vivo methods, currently limited to small nanoparticle clusters, produce self-assemblies in virus by electrostatic binding of metal ions at specific sites of the bio-engineered microorganism, followed by a reduction process (i.e., bio-mineralization)[2,19,20]. The clusters synthesized by all of the above-mentioned methods are small globules, non-percolating arrays, or multilayered films with percolation paths in three dimensions. Two-dimensional percolating monolayers of nanoparticles are possible using the organic cross-linkers with some success; however, the architectural control over the long range is difficult[21].

These percolating clusters of metal nanoparticles, in contrast to their micro-particle cousins, are fundamentally different in terms of the electrical properties due to the nature of inter-particle electron transport[22]. Because at nanoscale size, the charging energy to insert a single electron in nanoparticle is >1-10 fold the thermal energy, the inter-particle current flow is by single-electron transport as explicitly shown by transport studies on single-nanoparticle[23,24], their 2- and 3-dimesnsional assemblies[25-28], and single-nanoparticle devices (such as single-electron-transistor[29,30]). The above studies demonstrate that percolating cluster of metal nanoparticles is a viable unit to fabricate (single-electron) devices, where the micron-scale clusters will allow for easy-to-fabricate,

robust interconnection network for the nanodevice system. Because metal nanoparticles such as gold are stabilized in solution by electrostatic repulsion, forming a percolating cluster on physical substrates requires either an organic cross-linkers to stitch the particles[25,31] or polyelectrolyte to shield the charge of the particle[32,33]. For the biological substrates, the highly selective deposition relies on either highly specific binding (such as, DNA hybridization[16,34,35], biotin-streptavidin interaction[36]) or strong specific inter-molecular interaction (such as electrostatic interaction[37-39]).

Here we studied and developed a novel process to selectively deposit a percolating monolayer of Au nanoparticles on rod-shaped bacteria and polyelectrolyte fiber spanning between Au electrodes. Under an electric field between the electrodes, the electrons tunnel from one nanoparticle to another through a dielectric barrier formed by the polyelectrolyte coatings on nanoparticle from either the bacterium surface or the PAH fiber. We studied the electron-tunneling properties of these arrays and invoked a change in the electrical properties of the array by stimulating the bacterium or the PAH surface. This affects a change in the electron tunneling barrier characteristics, which is discussed in the following chapters. The intensity of electrostatic attraction was also studied using gold nanorod deposition, which led to bending of the rods to conform to the shape of bacteria.

The study of arrays of nanoparticles, where electron tunneling is the mechanism of transport, can provide avenues to develop complex devices that could work as memory, coulomb blockade, negative differential conductance and diode devices, operating at molecular level. Also demonstrated in this work is an electronic switch for memory storage, with a chemical/electrical device model to explain the observations. The

mechanism for high density self-assembly of the nanoparticles on bacteria and PAH fiber is also studied.

I believe that such a bio-material electronic hybrids will be an attractive concept to fabricate highly integrated electronic system requiring circuitry for power and signal on flexible plastic substrates using inexpensive beaker chemistry.

Nanoparticle deposition on Biomaterials

In this section, various methods to deposit pre-prepared nanoparticles to biological templates will be discussed. It will also be discussed how specific sites on biological templates can be used to nucleate nanoparticle growth[5,7,35,37-42]. Making metal nanoparticles by reduction of metal salts on such sites has been done on DNA, viruses, and bacterial S-layers. Ben-Yoseph and coworkers[16], constructed a DNA bridge and used the polyanionic nature of DNA to make silver nanowire on it. The DNA bridge was loaded with silver ions by Na^+/Ag^+ ion exchange using a 0.1M $AgNO_3$ aqueous solution with pH=10.5. The silver ion-DNA complex thus formed was reduced with basic solution of hydroquinone to form silver nanoparticles bound to DNA template. Further reduction leads to deposition of silver enough to form a conducting channel through the DNA. The silver particles formed ranged from 25-100 nm in size. The 25 nm sized nanoparticles did not cover enough DNA to form a conducting channel.

Mann and coworkers used Tobacco Mosaic virus as a template to make and deposit nanoparticles[2,3]. They deposited Pt, Au, and Ag nanoparticles on the virus. Platinum and silver nanoparticles of size smaller than 10 nm were produced on the surface of the virus, by reduction of $[PtCl_6]^-$ and $[AuCl_4]^-$ at acidic pH. They also used photochemical

reduction of Ag(I) salt at pH 7 resulting in nucleation and constrained growth of silver nanoparticles on the viral surface. For this method silver benzoate was found to increase the nanoparticle coverage on the virus more than silver nitrate. They used two stains of the virus, one with and the other without glutamic and aspartate acid. They found that the reduction of metal ions on the surface was a result of these acids present on the viral surfaces.

Sleytr et al, has shown that sites on bacterial S-layer can also be used to nucleate nanoparticles production by a similar technique mentioned above[43]. His group extracted the S-layer from *Bacillus Sphaericus* and chemically treated it to attach thiol groups to it. Then the S-layer protein was put in 10 mM solution of tetrachloroauric(III) acid for 4 days at 4^{o}C. It was found that the S-layer was completely covered with gold. Upon irradiation with electron beam, it was found that the gold accumulated on the pore region of the S-layer forming gold nanoparticles. These nanoparticles, 4-5 nm in size, were arranged on the S-layer with a repeat distance of 12.5 nm.

Batt and coworker made bacterial S-layers on solid substrates and deposited citrate capped nanoparticles on it[40]. For high ionic concentration, the nanoparticles on the S-layer were found to be separated by 18 nm, which is the pore-to-pore distance in the S-layer. For low ionic concentration, due to charge-charge repulsion between nanoparticles, the nanoparticles were found to be adsorbed on alternate sites on the S-layer. Sleytr et al., has also shown that the bacterial S-layer's specific sites can be used for deposition of positively charged nanoparticles of copper, silver and gold[42].

To attach pre-prepared nanoparticles on DNA templates, two approaches are used. One is the electrostatic attraction between the negatively charged phosphate groups on

DNA backbone and positively charged nanoparticle and the other is covalent bonding of functionalized nanoparticles with DNA. Maeda and coworkers mixed positively charged gold nanoparticles with DNA and kept overnight to observe binding on the nanoparticles with DNA[35]. They used 5 nm gold nanoparticles and found that the size of the Au-nanoparticle-DNA composite was 8 nm and concluded that the DNA was bundled. Sastri and coworkers modified Au nanoparticles, 3.5 nm in size, by attaching lysine to make it positively charged and attached it to negatively charged sites on DNA[37]. Ohtami et al., prepared gold nanoparticles by reduction of $HAuCl_4$ with aniline, capping the nanoparticle with positively charged aniline[38]. The 2 nm sized nanoparticles were then mixed with DNA to get a dense coverage of nanoparticles on the DNA. Similarly, Hutchison and coworkers prepared gold nanoparticles by $NaBH_4$ reduction of $HAuCl_4$ under phase transfer conditions in the presence of thiol terminated triphenylphosphine molecule[39]. This led to the formation of positively charged triphenylphosphine-terminated gold nanoparticles. These when deposited on negatively charged DNA produced gold nanoparticle 'ribbons'.

Willner et al., used covalent bond between DNA and psoralen to attach nanoparticles to DNA[41]. Gold nanoparticles functionalized with N-hydroxysuccinimide were modified by mixing with amino psoralen to form gold-nanoparticle-psoralen complex. This was then added to DNA solution and exposed to 12 W UV light ($\lambda > 360$ nm) for 45 minutes to covalently attach gold nanoparticle to DNA. Recently Yan and coworkers attached streptavidine-Au-nanoparticle conjugate to attach it to DNA[36]. This method can leads to specific attachment of the nanoparticles on the DNA. Other than the covalent bond formed between the DNA and the gold another advantage of this method is

that because of the positively charged streptavidine, the interaction between the nanoparticle and DNA is high.

3. FABRICATION OF BACTERIAL DEVICE

In this section, the fabrication process for gold nanoparticle/bacterial hybrid device will be discussed. The various steps involved and process characterization for controlled deposition of gold nanoparticles on the bacterial surfaces will be shown. This process is only for gram-positive bacterium.

It will be shown that gram-positive bacteria are viable scaffolds for deposition of metallic nanoparticles, and that the rich electronic characteristics of the nanoparticle-array could be used to make highly functional devices. A single step deposition process will be shown to be effective enough to deposit a percolating and conducting monolayer of nanoparticles. It will also be shown that the system overcomes the inter-particle electrostatic repulsion, to build a percolating monolayer. The preliminary data on the electronic properties of metallic nanoparticle array will be discussed. In the next chapter it will be shown that subtle movement of the nanoparticles induced by 'electrical annealing', can be used to make an electronic memory device. Also humidity sensor application of this device will be discussed in Chapter 5. The current Chapter will provide information on the fabrication and characterization of the bio-hybrid device.

3.1 Poly-L-Lysine coating on gold nanoparticles

This section explains the coating of positively charged Poly-L-Lysine on negatively charged nanoparticles. This coating is performed using a low molecular weight Poly-L-Lysine with degree of polymerization of < 20. The positively charged Lysine coats the negatively charged gold surface by specific electrostatic interaction. The theoretical concentration for 100% coating with Poly-L-Lysine with an area of ~ 10 A^2 can be easily

calculated. The concentration of Poly-L-Lysine that produced a stable solution though, was thousand times more than this theoretical value. Lesser concentration leads to an unstable solution, which agglomerates very fast. The reason for this agglomeration is that during the relatively slow coating process, the nanoparticles do not immediately get coated with lysine. As a result, there are regions on the nanoparticle, which are not coated and are still negative. These negative sites are attracted to nanoparticles covered with positively charged Lysine. This leads to agglomeration of particles and the solution becomes unstable. Therefore, all the particles have to be completely coated before new negatively charged particles are exposed to lysine. Therefore, what is done is that Lysine solution is first prepared and the nanoparticles are then slowly added to it. The excess Lysine does not allow any negative sites on the nanoparticle. This reduces the possibility of agglomeration leading to a stable solution. The excess lysine is left in the solution and does not interfere with the experiment, as will be explained later. Therefore, all the nanoparticles get positively charged and coated with Lysine, with minimal agglomeration. The solution remains stable for about 7 days.

3.2 Deposition of nanoparticles on bacteria

Based on the observations shown above, a protocol was developed for deposition of nanoparticles on the bacterium. The steps involved are shown in Figure 1.

Bacteria Preparation

Bacillus Cereus (ATCC 21364) was cultured in 8 gm/ml autoclaved nutrient broth (difco) media, at 30^{o}C. After 14 hours of incubation, the bacteria reach log-phase in its growth. It was found, that at this stage, the bacterial affinity for Lysine was maximum.

This was found by making different aged bacteria and depositing them on lysine coated surface. The bacteria are then centrifuged and washed with autoclaved DI water three times after which, the bacteria are resuspended in sterile water.

Chip Preparation

A typical Silica-electrode chip has a Silica depth of 100-500 nm with gold electrodes 7 ± 0.2 micron apart and 5-10 mm in length. Each chip has 20 sets of such electrodes. The chip is cleaned in oxygen plasma followed by high DP (degree of polymerization) Lysine coating. The chip is then put in the freshly prepared bacterial solution for 10-15 min. Usually 20-50 bridges are formed for every device. The extra-cellular polymeric substances (EPS) is removed from the bacteria by washing the chip in a 2N NaOH solution for 1 min. (The effect of EPS will be shown in the section 3.3). The bacteria deposited chip is immediately put in lysine coated gold nanoparticle solution. This solution with pH of ~ 7 has 1 mg/ml of DP 4 lysine (2000 Daltons) and nanoparticle size of 30 nm. The nanoparticle deposition is achieved in 8-12 hour. The deposition density is discussed below.

A highly controlled deposition of nanoparticles is achieved by regulating the deposition time in the Au nanoparticle solution (see Figure 2(a) to (e)). Since both the Au nanoparticles and the substrate are positively charged, the deposition is highly selective with a monolayer formation only on the (negatively charged) bacteria surface. However, the negative surface charge is not the only reason for the electrically percolating deposition. Figure 2(f) shows deposition of the same Au nanoparticles on a negatively

charged "physical surface" prepared by adsorbing monolayer of poly(sulfonated styrene) (70,000 Daltons with <90% sulfonation) on the lysine coated SiO_2/Si substrate (described

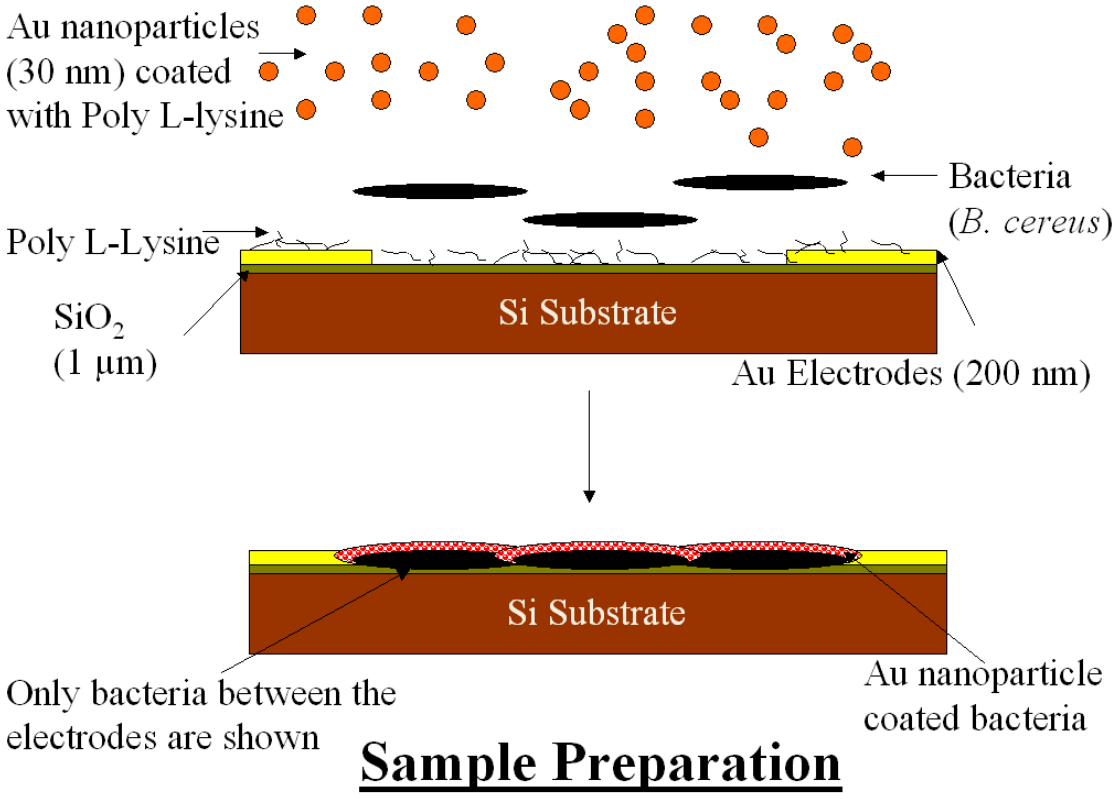

Figure 1: Sample-fabrication steps involved in coating the bacteria with nanoparticles. Gold nanoparticles with positively charged Poly-L-Lysine coating deposit on negatively charged bacterial surface.

above). Multilayer deposition of nanoparticles is self-inhibiting because of inter-particle columbic repulsion. Since silica surface is also positively charged because of the lysine coating, no particles deposit on it.

The SEM images below (Figure 3 a and b) show bacteria coated with nanoparticles spanning between the two electrodes and a high-resolution image showing a good contact

of the nanoparticle array with an electrode. This confirms that the contact resistance of this device will be very less.

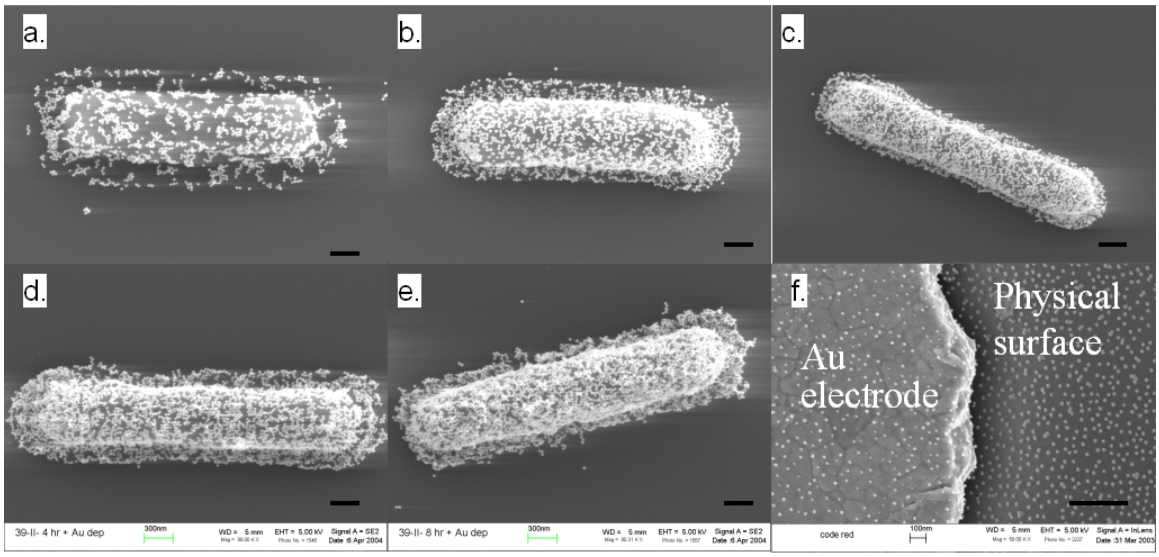

Figure 2: Highly controlled, highly selective deposition of Au nanoparticle on bacteria: Lysine coated 30 nm Au nanoparticle deposition from pH 7 solution for (a) 30 min, (b) 1 hr, (c) 2 hr, (d) 4hr, and (e) 8 hr. (f) Same (positively charged) Au nanoparticles are deposited on a (negatively charged) PSS coated lysine/SiO_2/Si substrate for 16 hrs. The Au nanoparticles are percolating after 4 hr. deposition on bacteria while no conduction is observed for the physical surface in (f). Bar size = 300 nm. The small amount of multi-layer formation for high deposition time is due to contraction of the membrane because of loss of water in Scanning Electron Microscope.

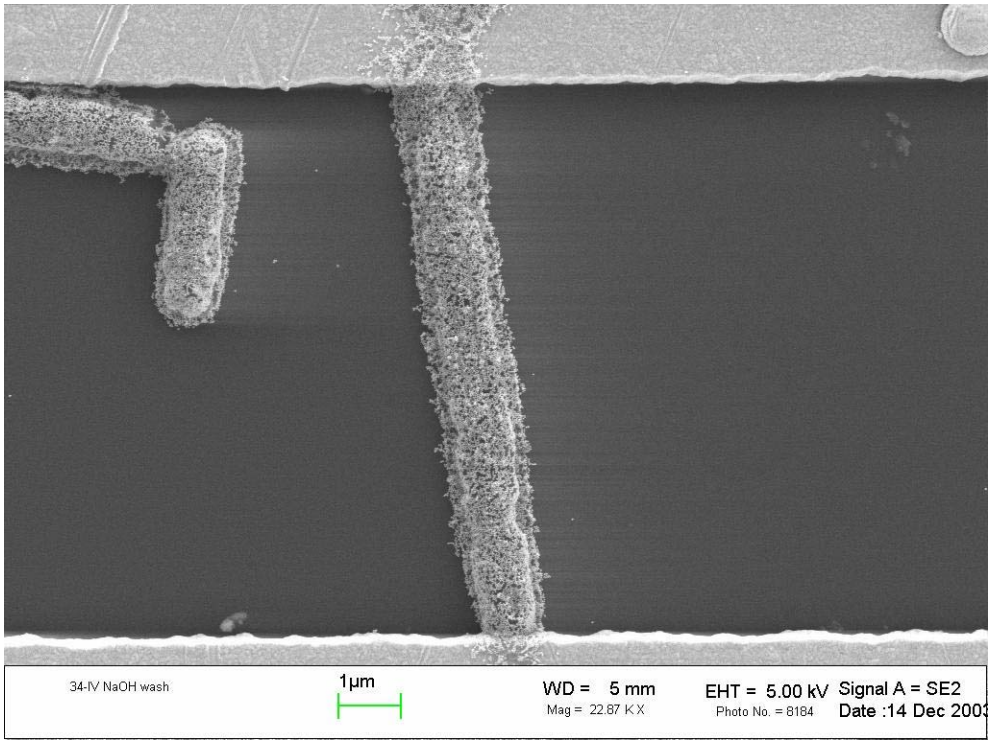

a.

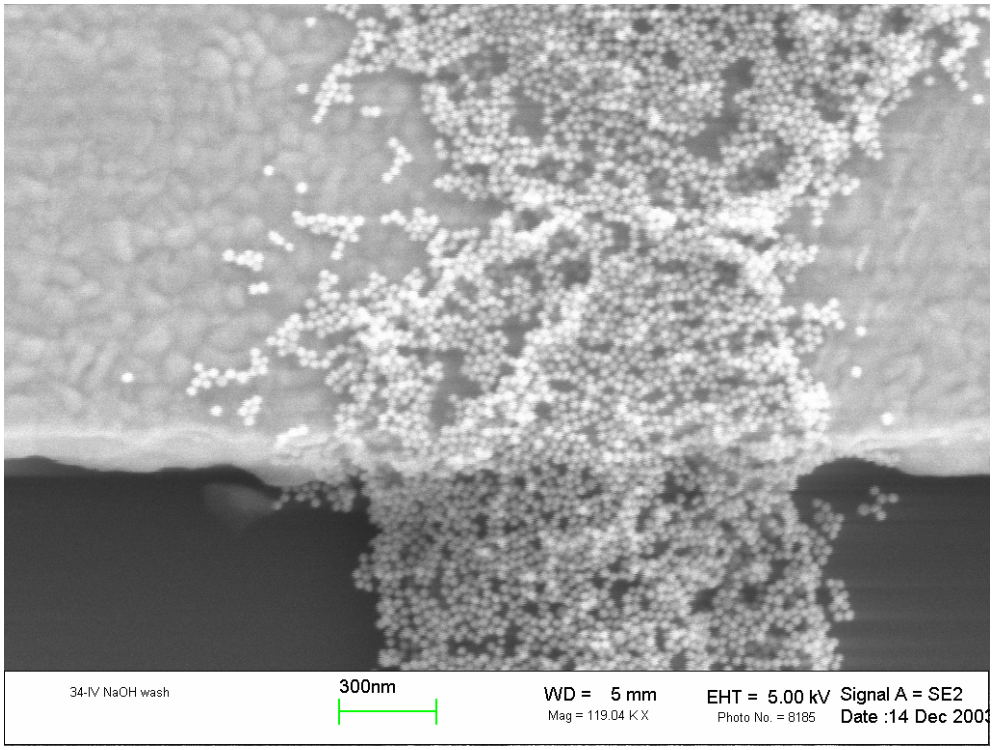

b.

Figure 3: (a) Typical FESEM image showing the bacteria spanning between two Au electrodes at the extreme ends. The bacteria are coated with monolayer of 30 nm Au nanoparticles more clearly evident at higher magnification shown in (b). (b) also shows the good nanoparticle contact with the gold electrode.

3.3 Is Bacteria live or dead?

A standard assay of PI/SYTO 9 dye is used to confirm the fate of the bacteria[31] after the deposition process. The green coloration in Figure 4 shows that the bacteria survive the complete device fabrication process. Because integrity of the peptidoglycan surface membrane in which the teichoic acid molecular-brush is imbedded is critical for the Au nanoparticle deposition, the survival of the bacteria for the device fabrication is important. Any lysis of the bacteria (or release of extra cellular polymeric substances - EPS and/or internal bacterial fluids) will lead to ill-formed, non-functional devices. The bacteria survive the process of lysine coated nanoparticle deposition due to the bacterial affinity to lysine, which is a nutrient to the bacteria.

Also, one of the most important steps in this process is the NaOH wash just before the nanoparticle deposition. It was observed that without NaOH wash, nanoparticle coverage suffers. The extra-cellular polymeric substances (EPS) excreted by the bacteria leads to regions on its surface that are not negatively charged. EPS is excreted form bacteria as a defense mechanism. The samples without NaOH wash did not produce well-formed monolayers. If the bacteria are put in DI water for a long time, it apparently gets threatened and produces EPS. This EPS then deposits on the surface of the bacterium and covers the negative charge on the bacteria leading to lesser nanoparticle deposition. Figure 5 shows the coverage of nanoparticles after the bacteria is put in DI water after NaOH wash. The figure shows, that the nanoparticle coverage deteriorates as the bacteria is exposed more and more to DI water. This is a proof that bacteria although immobilized, still interact with the environment, and are therefore alive.

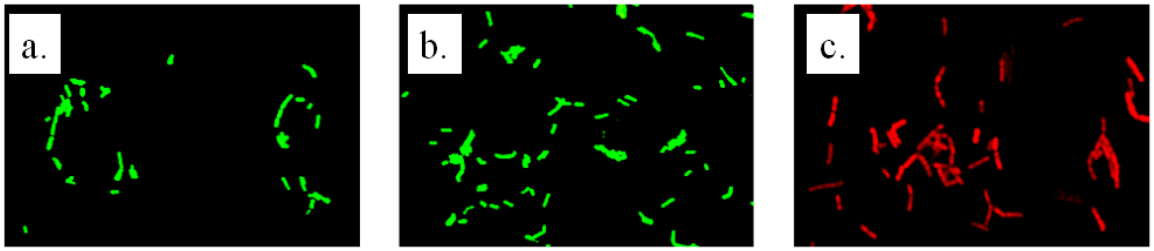

Figure 4: The fate of the bacteria during device processing: The standard PI/SYTO 9 assay is used to probe the survival of the bacteria at various stages of the process. Confocal microscopy of different samples at following stages is shown: (a) Bacteria immediately after immobilization from the nutrient broth on the substrate; (b) after the gold nanoparticle deposition for 4 hrs.; and (c) after 10^{-5} torr vacuum for 2 hrs. The green and red coloration indicate that the bacteria are alive and dead, respectively.

The polyelectrolyte on bacterium surface, i.e., the teichoic acid, is a flexible brush, and is tethered to the peptidoglycan surface at one end with rest of the chain in high thermal motion (i.e., high mobility (see appendix)). Furthermore, because the brush contour length is typically ~ 18 nm[29], it is reasonable to expect that the negatively charged teichoic acid molecule with high mobility and chain flexibility may wrap over the positively charged Au particle up to a maximum possible subtended angle of 135^{O} from the point of contact to minimize free-energy. A similar screening of charge by PSS would be difficult in the case for PSS/Poly-L-Lysine structure due to restricted mobility. Specific attachment of Concanavalin-FITC dye to the teichoic acid[30] followed by confocal microscopy confirms their uniform distribution of the brush on the bacterium.

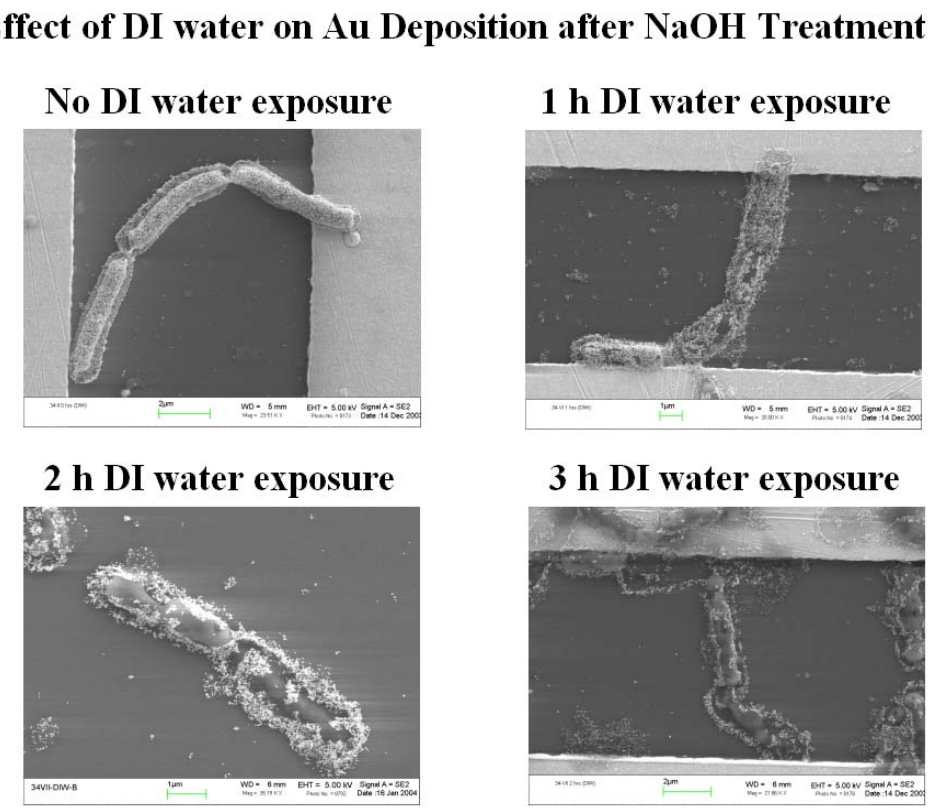

Figure 5: Effect of D.I. water exposure on nanoparticle deposition on bacteria. As the D.I. water exposure time is increased, EPS releases more and covers the negative charge on the bacteria leading to decrease in nanoparticle deposition.

Because, no nanoparticle deposition on the bacterium occurs subsequent to the neutralization of the teichoic acid after the attachment with Concanavalin, the role of the latter in high-density deposition is justified.

Bacillus cereus was found to have the best affinity for lysine coated nanoparticles when it was in the logarithmic stage of its growth process, which is ~ 14 hrs in nutrient broth at 30 ^{o}C. After 72 hours of growth in nutrient broth, the bacterial affinity for lysine was found to have degraded. This may be attributed to the lag-phase of growth where the bacteria start dying. Autoclaved bacteria also lost their affinity to lysine. After

autoclaving and filtering the bacteria, they were not able to adhere to lysine-coated silica. The small number of bacteria that did adhere did not produce percolating nanoparticles clusters.

The deposition of nanoparticle on PAH polyelectrolyte fiber will be discussed in Chapter 7.

4. MEMORY DEVICE ON BACTERIA

Current-Voltage (I-V) Curves

The current-voltage measurements were made using Agilent 3458A digital multimeter and Agilent 6614C power supply. The measurements on device showed slightly non-linear curve as can be seen in Figure 6. There was no threshold coulomb blockade voltage, as observed in the case of 1-D nanoparticle arrays[44]. The non-linear curvature although, is a signature of coulomb blockade where, there is a repulsive force experienced by electron entering a nanoparticle already charged with an electron. As the current increases the number of electrons passing through a nanoparticle increases. This reduces the residence time of electrons in that nanoparticle, and therefore there is less repulsion to the next electron entering the nanoparticle. Therefore, the slope of the IV curve increases as the current increases. When there is a coulomb blockade threshold, there is no conductivity before a certain voltage. As the size of the nanoparticle becomes small, the capacitance (= $4\pi\varepsilon r$) reduces and the charging energy = e^2/C, increases. This increase in charging energy leads to zero conduction below voltage of e/2C. This voltage is known as coulomb blockade threshold. In our case, since the nanoparticles are 30 nm in diameter, the coulomb threshold is expected to be very small, and at room temperature, the thermal motion of the electrons will fade it.

In the IV, there was a small hysterisis, which was found to diminish as more and more measurements were taken as seen in Figure 6. The curves were found to become more and more linear with measurements too as depicted by regression (R^2) values. The measurements were taken by a triggering process, which does not expose the voltage applied for more than 0.1 s.

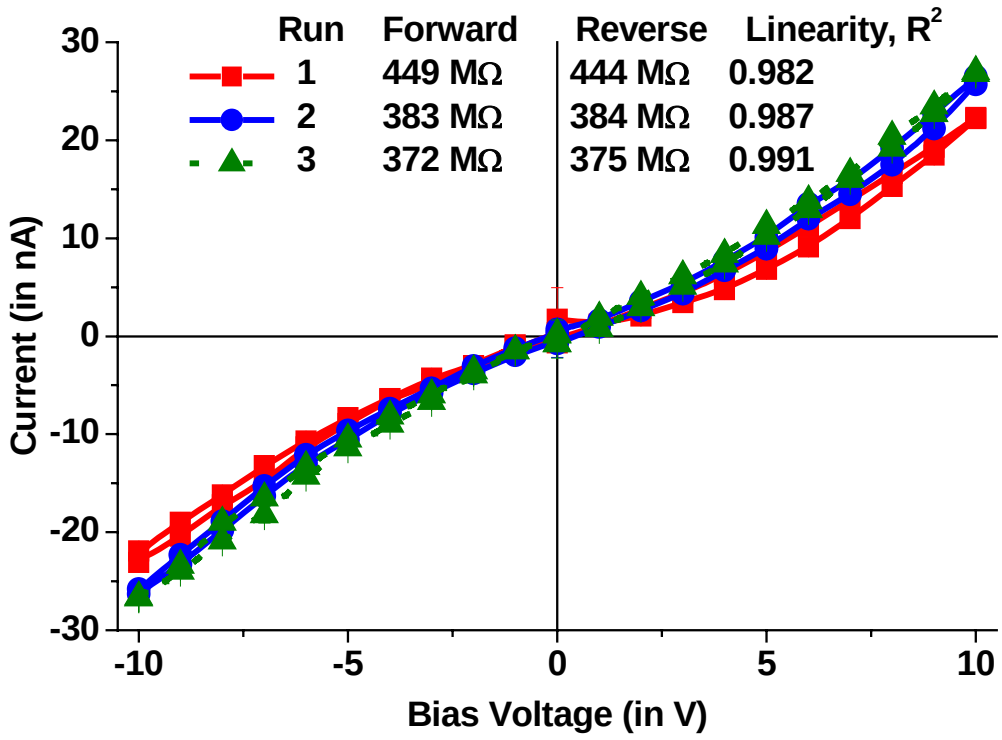

Figure 6: Typical *I*-*V* characteristics of as-received (run #1) and subsequent cycles of a device with 15 bridges between the electrodes. The error bars on each data point are based on 10 points over a time period of 5 s. The resistance is measured by fitting a line through the origin with fitness parameter R^2. The *I*-*V* characteristics become reproducible after the first run.

Voltage annealing process

The device could also be 'voltage annealed' to increase the conductivity of the nanoparticle network. In the annealing process one electrode is subjected to a high potential (–50 V), while the other electrode is kept open. The conductivity is measured after every 2 mins of annealing. The normalized conductance increases with annealing time. It is expected that this effect is because of the image charge effect. It is well known that there is always an attraction between charged species and metal. Therefore charge accumulation on an electrode due to applied potential attracts the metal nanoparticles.

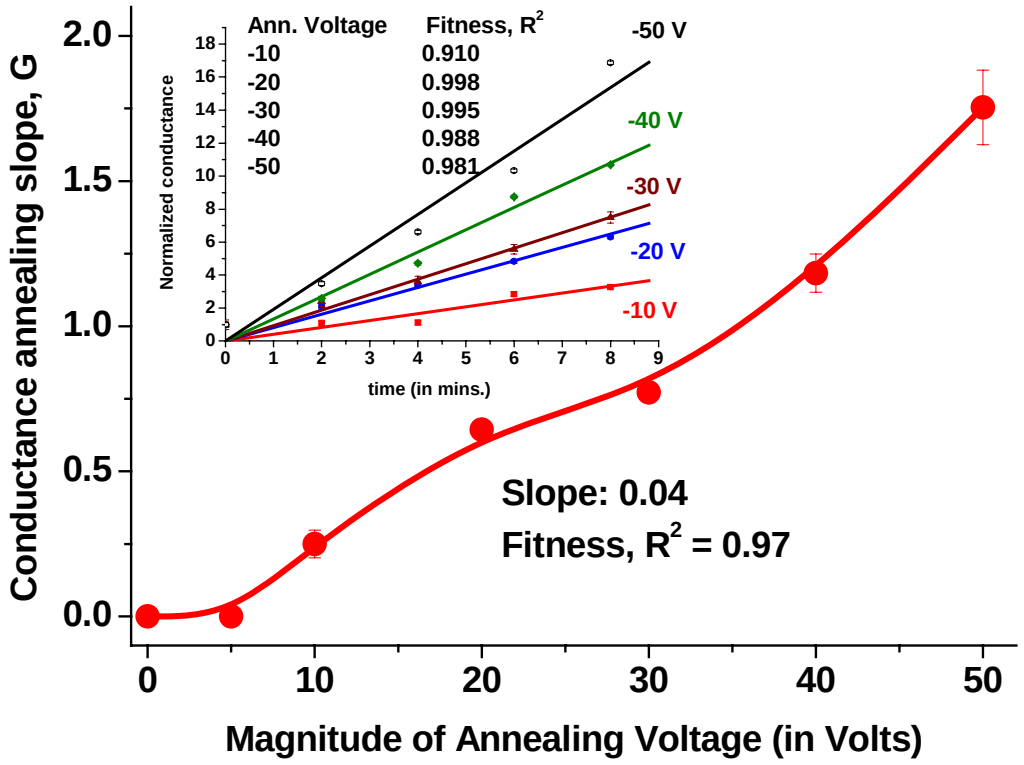

Figure 7: Normalized conductance is defined as R_i/R, where R_i is the resistance at t = 0 (i.e., after the third cycle in Figure 1). All the devices are on the same chip and therefore fabricated under identical conditions. The slope G is in min^{-1}.

The nanoparticles which are not well connected to the electrode or other nanoparticle clusters, will therefore be attracted, leading to more conductive pathways. This will result in an increase in the conductivity of the system.

The conductivity increases linearly first and then flattens out. In the linear region the slope of normalized conductivity and time is directly proportional to the annealing voltage as can be seen in Figure 7.

Since the morphology and conductivity of the device is a function of the bacterial age, all the measurements shown were made on different devices on the same chip. A

threshold voltage of –5 V is observed before the annealing starts. This threshold is believed to be due to mobility barrier caused by good adhesion between the nanoparticles and bacterial surface.

The increase in conductivity due to an increase in the number of conductive pathways can be explained as "electrodeposition" of Au nanoparticles on the "live cluster" that is connected to the electrode at V_O. The diagram below shows the decrease in relative resistance with annealing time. The conductivity can increase by three mechanisms. (i) Conductivity can increase as a result of a decrease in contact resistance between the percolating cluster and the electrodes. This possibility is ruled out because, on an annealed device, applying negative potential on the other electrode does not increase the conductivity by a lot. (ii) The existing percolating channels widen during the electro-deposition process leading to concomitant increase in conductivity. Such coarsening of the channels should lead to striated morphology along the field direction. Since no distinctive change in morphology is observed in FESEM well after the conductance saturates, this process is not significant. (iii) Subtle movement of the particles leading to increase in branching of the percolating network increases the number of parallel pathways.

Possibility (iii) is explored by considering a simple model. We start with a single channel spanning between the electrodes as shown in the inset of figure. The channel is a necklace of nanoparticles with a constant intrinsic resistance per length. From earlier figures, it is evident that the area-coverage of the particles is well over the percolation threshold. Furthermore, the measured *I-V* characteristic is a combined effect of ~15 bridges between the electrodes. Thus, on average due to annealing, we assume that the

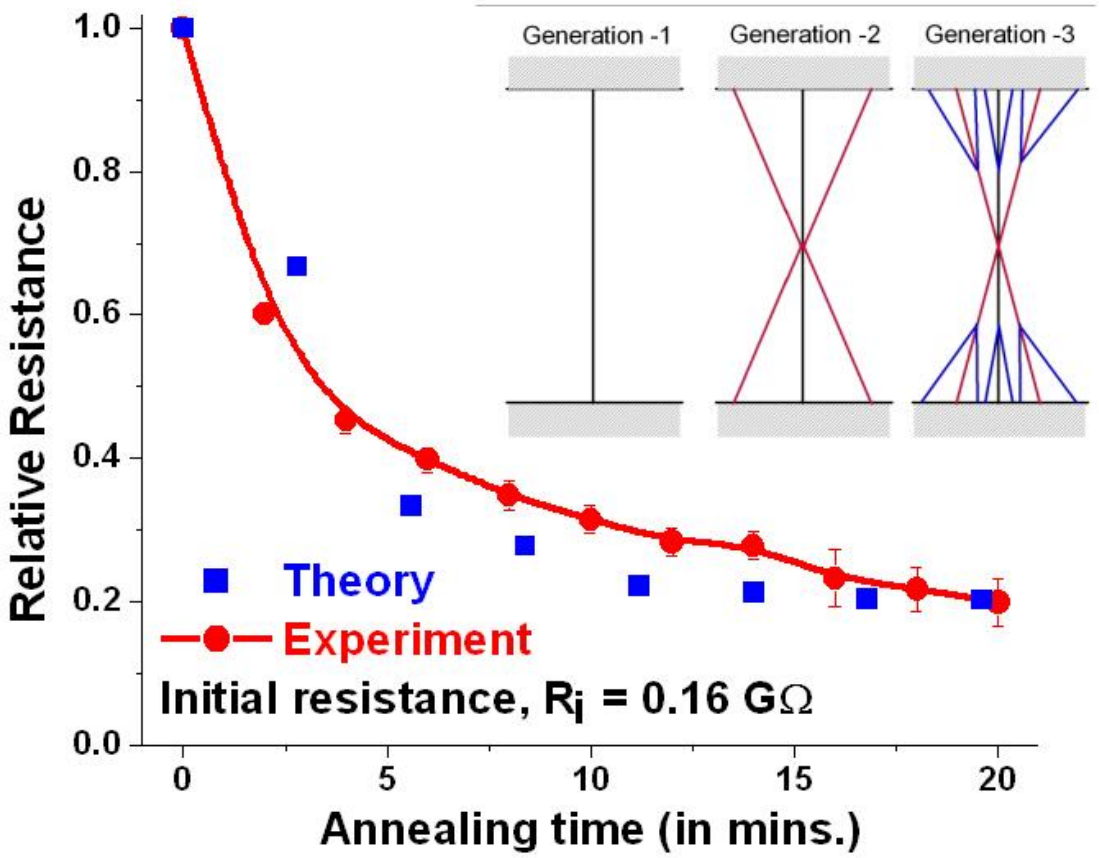

Figure 8: Annealing time versus relative resistance, R/R_i of a sample showing the plateau region after ~ 20 min. The theoretical points are based on the percolation model for coordination number, $f + 1 = 4$. Inset shows three generations due to $f = 3$ branching. The channels are drawn as straight lines for simplicity.

channel bifurcates at the center into *f* branches as shown in generation-2 of inset Figure 8 above (for $f = 3$). As the electro-deposition progresses, the sub-branches bifurcate further at the center to form a generation-3 structure. Owing to averaging over large number of channels, the bifurcation is assumed to progress at constant intrinsic channel resistance and invariant *f*. The relative resistance for generation-*n* is a simple analytical function:

$$\frac{R(n)}{R(1)} = \frac{f\left[(2f)^{n-2}+1\right]-1}{f\left[2f-1\right](2f)^{n-2}} \qquad 1$$

where, $R(1) = Ri$. The normalized resistance at time$\rightarrow\infty$ is given by, $R_\infty/R_i = 1/(2f-1)$. For data in Figure 11 above, $R_\infty/R_i = 0.2$, implying $f = 3$. Using a constant time interval between the various generations (the only fitting parameter), from above equation, change in relative resistance as a function of annealing time is calculated. As shown in the Figure 8, the agreement between the model and the experiment is reasonable. An analytical expression is obtained with off-midpoint bifurcation. Although the adjustable offset parameter improves the model-experiment agreement, no significant new information is gained. More complexity is introduced by using a distribution of generations at $t = 0$. Again, the fit improves; however, the underlining mechanism remains invariant, i.e., occurrence of successive branching of percolating channels due to annealing.

5. HUMIDITY SENSOR ON BACTERIA

This section describes another very fascinating application of this system, where this electronic device can be used as a humidity sensor. The response of the system is shown in the Figure 9. The inset shows a typical Au nanoparticle monolayer coated bacterial bridge connected to the Au electrodes. One bridge constitutes a device. All the current-values are normalized by number of bridges between the electrodes and were measured at 22 ^{O}C. Figure 9 shows the normalized current, I, between the bridges as a function of relative humidity R_H. The Au nanoparticle deposition is optimized for 4 hrs. (see Figure 2(d)) to obtain the largest change in current due to humidity. Figure 9 indicates that the device behavior is reversible and stable over a slow run taken over ~40 min. per cycle. Because of complete reversibility of the device, it is unlikely that the water inside the bacteria plays any significant role. In contrast to most impedance based microelectronics humidity sensors[45], the resistance of the device decreases as humidity increases. The largest change in current, and hence highest sensitivity, is for the low humidity region of $R_H < 20\%$.

A simple model based on Figure 10 explains the observation in Fig. 9. As the humidity increases, the peptidoglycan membrane absorbs water. Assuming no excess volume of absorbed water, the volume fraction of water absorbed is fR_H, where f is Henry's constant. Assuming affine swelling of the peptidoglycan membrane, the linear extension of the membrane due to absorption is $(1-fR_H)^{-1/3}$. Because the nanoparticles are fixed on the membrane, the interparticle separation is given by, $a/a_O = (1-fR_H)^{-1/3}$, where a_O is the separation at $R_H = 0$. Because electron tunneling is the primary transport mechanism, the current is given by Fowler-Nordheim equation[46].

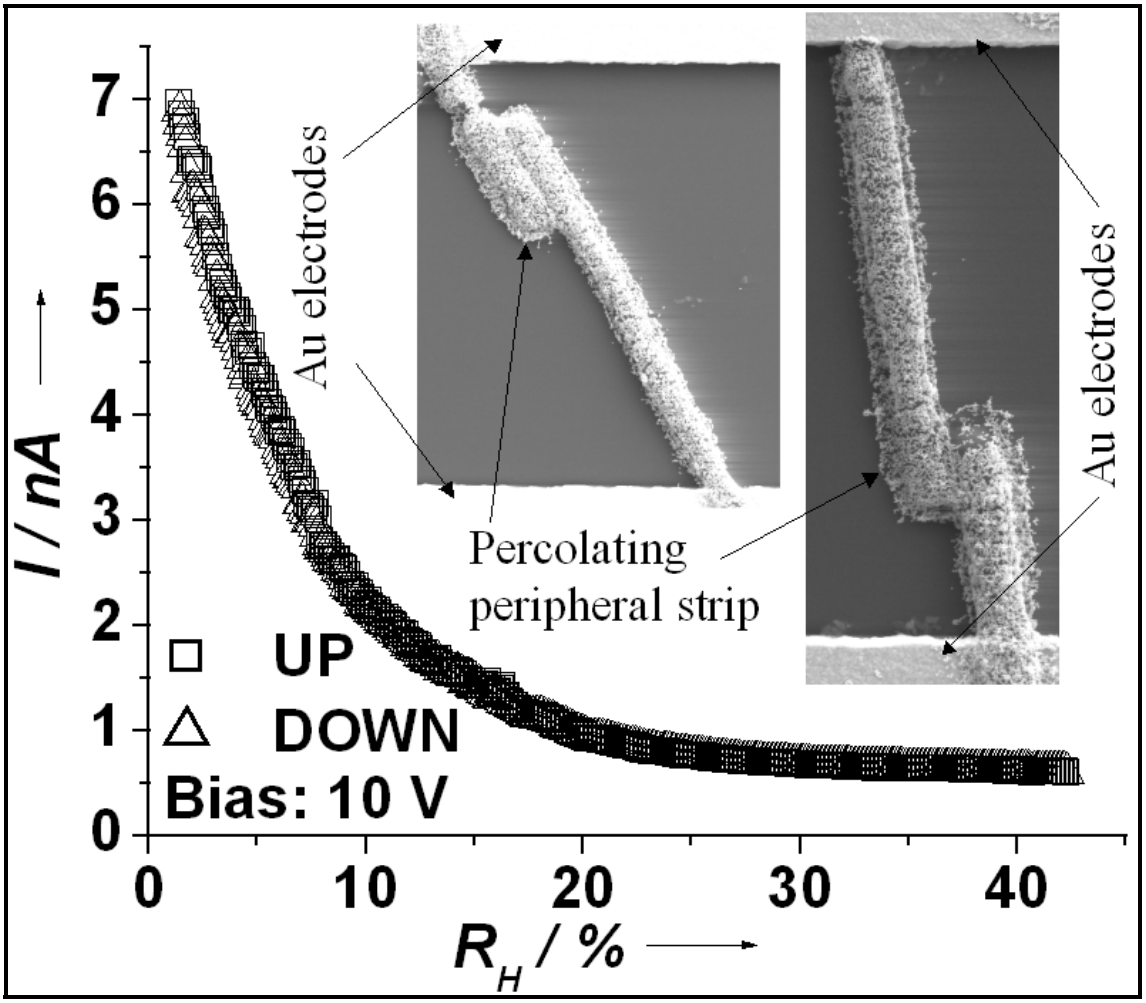

Figure 9: The characteristics of the humidity sensor: Typical device current (*I*) as a function of relative humidity (R_H) for "up" (i.e., humidity decreasing) and "down" cycles at a bias voltage of 10 V. The current is normalized per bridge. The inset shows two typical bacteria bridges spanning between the electrodes. The peripherals strip is a (percolating) monolayer deposition of nanoparticle.

Using the wave function of the electron, the electron tunneling current through a barrier between two nanoparticles is given by: -

$I = I_o \exp\left(-2\alpha \sqrt{\frac{2m(V_o - E)}{\hbar^2}} \right)$, where, I_o is proportionality constant, E is the applied electric potential, V_o is the potential barrier and α is proportional to the inter-particle distance.

For thermionic emission (field assisted emission) from a surface of a metal the equation for current density is by Richardson Dushman equation, given below.

$J = B_o T^2 \exp\left(\frac{-\left(\phi - \beta_S E^{1/2}\right)}{kT} \right)$, where $\beta_S = \left[e^3 / 4\pi\varepsilon_o\right]^{1/2}$ (= 3.79 X 10^{-5}) is the Schottky coefficient. For electron passing thermionically through a gap, the probability of emission at a temperature is given by $P \approx \exp\left(\frac{-2\left(2m_e\phi_{eff}\right)^{1/2} x_F}{\hbar} \right)$, where x_F is the width of the gap and, ϕ is the effective barrier height. For our system, combining the electron tunneling equation with the Henry's law gives us: -

$$I = \left\{ \frac{V}{R_0} \exp\left[-\frac{Ka_0}{\sqrt[3]{(1 - fR_H)}} \right] + \frac{V}{R_B} \right\} \quad (1)$$

where, $K = (32\pi^2 m_e \phi / \hbar^2)^{0.5}$ (h is Plank's constant, m_e electron rest mass, and ϕ is the barrier height at nanoparticle/organic interface (work function)), R_B is the resistance to the leakage current from the peripheral as shown in Figure 9, R_0 is a normalization constant proportional to device resistance at $R_H = 0$, and V is the bias across the device (i.e., bacteria bridge). It is conjectured that the peripheral strip leading to finite R_B is due to deposition of proteinaceous substances secreted by the bacterium (for adhesion to the substrate). To decipher the effect of water absorption by poly-L-Lysine on the device

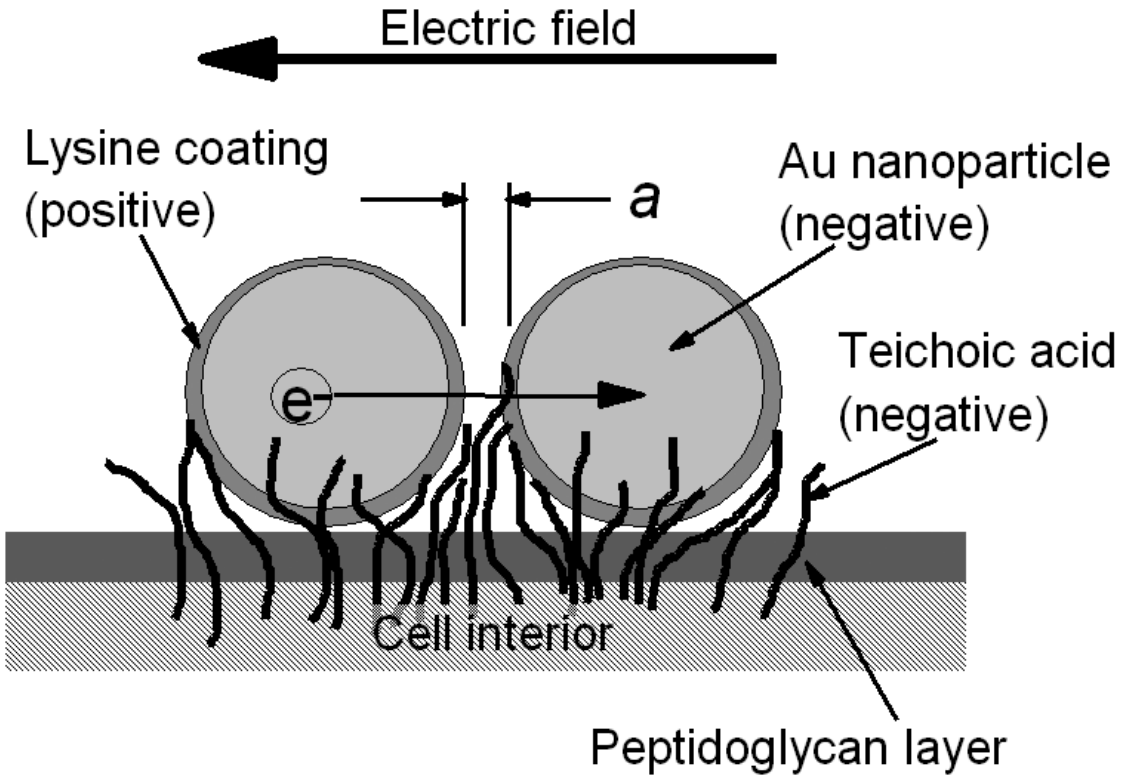

Figure 10: Schematic of the closely packed nanoparticle: Schematic showing two poly-L-lysine coated Au nanoparticles clutched by negatively charged teichoic acid molecules. The distance between Au nanoparticle surfaces is *a*. The electron transport from right to left is through a mixture of organics (lysine, teichoic acid) and air. The role of the electric field inducing electron transport is discussed later in Figs. 4 and 5.

performance, after the device fabrication, we capped the amine groups of poly-L-Lysine with glutaraldehyde to reduce the water uptake by Lysine. No significant change in device performance was observed indicating that the role of moisture absorption by poly-L-Lysine on device performance is negligible.

Figure 11 shows the fit of the experimental observation to eq. (1) (for the same device) at different *V*. Each excursion in humidity was ~ 40 min. long and the lapse between consecutive runs on average was ~1 hr. Although eq. (1) has four fitting parameters, the validity of the model is justified because they are reasonably constant

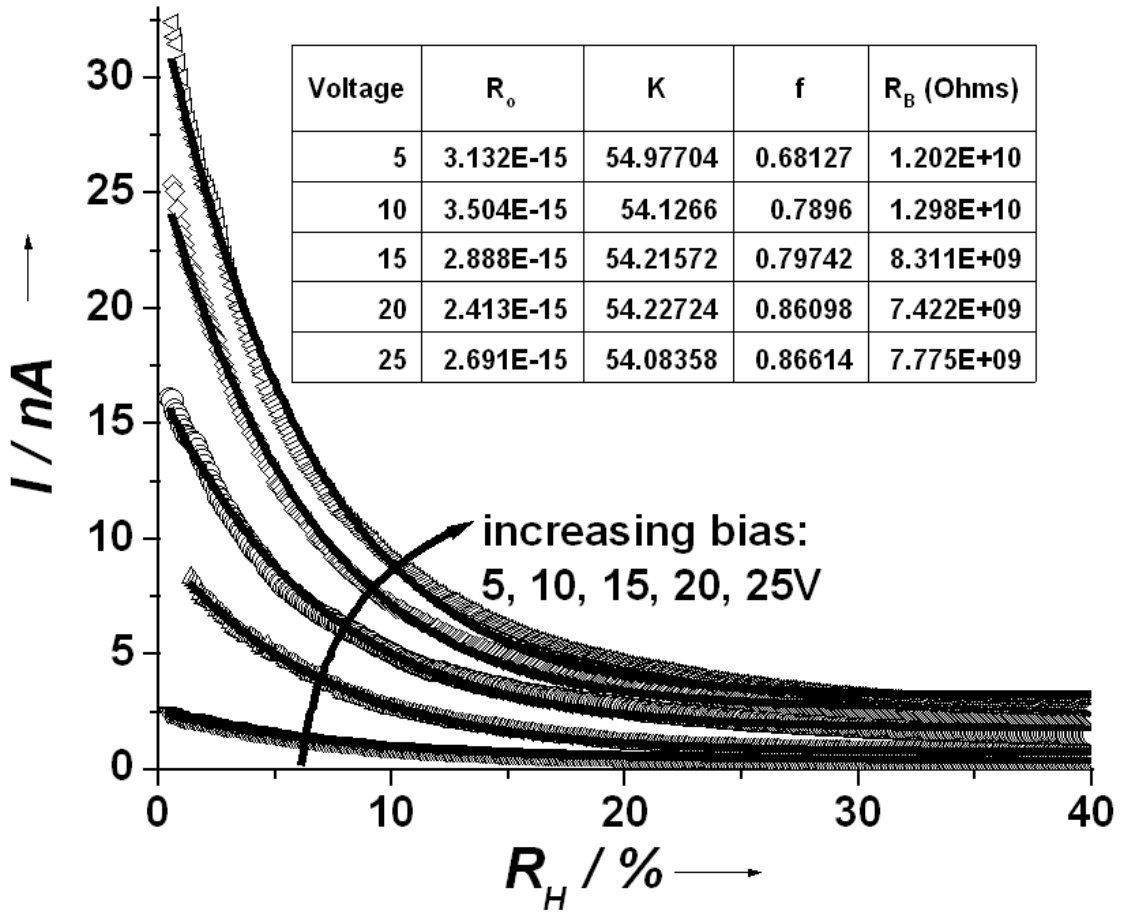

Figure 11: The validity of model and Peptidoglycan actuation: (a) The comparison of theory (solid lines) in Eq. (1) and experimental observation (data points), for current (*I*) versus relative humidity (R_H), are compared at various bias for the same device. The consecutive measurements on the device are made at increasing bias, i.e., 5, 10, 15, 20, and 25 V. The solid line and discrete points are theory and experimental data, respectively. The inset shows the four fitting parameters, K, f, T_0 and R_B.

over all the biasing voltages (see Table in Figure 11). The constant R_B implies ohmic behavior (independent of R_H) for leakage current given by, $I_B=V/R_B$. This is reasonable because on the peripheral region, the nanoparticles are not on the peptidoglycan membrane but adsorbed on to proteinaceous corona of the bacteria that does not change significantly in the lateral dimension due to humidity. Because, the contact resistance is not expected to be large[7] and is a strong function of humidity, it is included in R_B. We

also note that because the current through bacteria-bridge with no nanoparticles is insignificant, ionic currents can be neglected.

Figure 11 shows the corrected current, $I - I_B$ that flows through the nanoparticle monolayer as a function of percent change in inter-particle separation (estimated from *f*). Interestingly, for a humidity change from 20 to 0% corresponding to calculated decrease in inter-particle distance of only 7%, the (corrected) current increase by over 40-fold. Because the corresponding increase in total current, *I*, is only ~7-fold (see Figure 11), a reduction in peripheral deposition will improve the device sensitivity significantly. It will be shown that in the case of polyelectrolyte fiber, there will be no peripheral deposition and therefore no leakage current (Chapter 8). The high sensitivity to subtle change in interparticle distance is attributed to transport by single-electron-tunneling through the percolation network because the charging energy $e^2/(2\pi\varepsilon\varepsilon_0 D) \sim 1.5kT$ (where, $\varepsilon \sim 3$ is the dielectric constant of the organic coating and *e* is electron charge). Using the model parameters, and a tunneling barrier of 5.1 eV (i.e., *a* is much larger than poly-L-Lysine coating thickness in Figure 10 implying metal(poly-L-lysine)/air/metal(poly-L-Lysine) junction), the nanoparticle separation at 0 % humidity is ~ 2.3 nm, implying an absolute change (for 0 to 20% humidity range) of < 0.2 nm. We note that the sensitivity is significantly lower for devices fabricated at deposition time ≥ 8 hrs, where ohmic *I-V* is observed[7] than the non-ohmic behaviour for 4 hrs. deposition time device (see inset of Figure 12). On the other extreme, for deposition time of 2 hrs. the inter-particle distance in the contiguous clusters is too large for significant tunneling current. Thus, a combination of exponential dependence on *a* and $a \sim 2.3$ nm explains the high sensitivity of the system. Furthermore, in contrast to the earlier reports on Au/organic composite

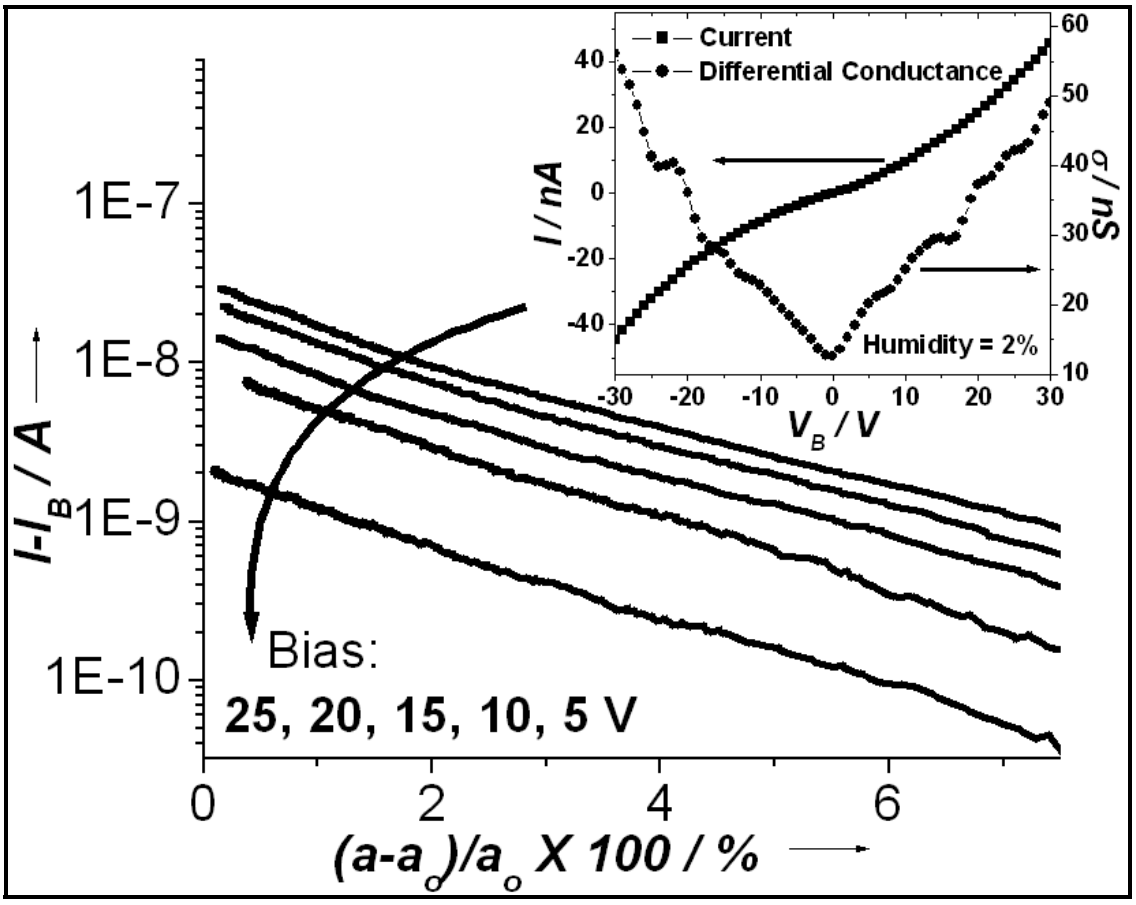

Figure 12: The Figure shows the corrected current, I-I_B, (after subtracting the calculated leakage current, I_B) as a function of calculated percent change in inter-particle distance, a, due to humidity induced dimensional change in the peptidoglycan membrane. Consistent with the model (Eq. (1)), the straight line for all biases in the semi-log plot indicates exponential dependence. The inset shows the (non-ohmic) I-V characteristics and differential conductance, σ.

thin-film sensors[47-49], where electron transport is by thermionic-emission or activated-tunneling, in this case, electron transport is via tunneling because the activation energy for tunneling is ~1.7 meV (see Figure 13) which is much smaller than free-electron's thermal energy, $kT \sim 25$ meV at room temperature.

This activation energy measurement was made after installing a low temperature liquid Helium chamber. The chamber has a 'cold finger' attached to liquid Helium source

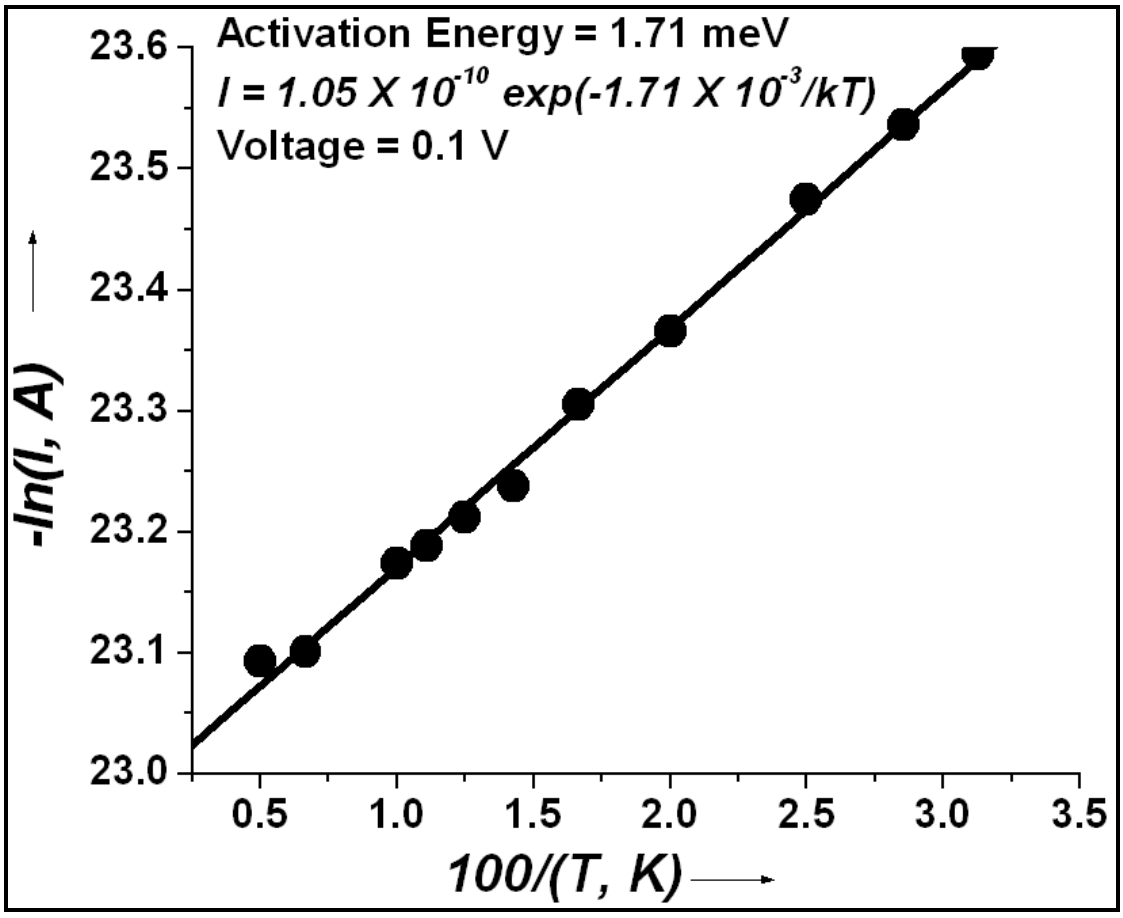

Figure 13: Temperature dependence of the device current at 0% humidity: Plot of negative of natural logarithm of current I, versus 100/T with applied bias of 0.1 V. The units for I, T and *kT* (for the formula in the in-set) are A, K and eV, respectively.

with a heater to control the temperature. The whole chamber is attached to a vacuum pump (and Turbo pump), which pumps down the system to 10^{-6} Torr. The samples are mounted on the 'cold finger' with electrical feed-through for IV measurement.

This process and the system can therefore be used to fabricate an active hybrid bio-electronic device using "physical" nanomaterials and a live microorganism. Here the electrical property of the monolayer of nanoparticles is controlled by actuating the peptidoglycan layer of the bacterium. A < 8% actuation in the peptidoglycan membrane,

induced by humidity excursion from 20 to 0%, leads to > 40-fold increase in the tunnelling current.

6. USING NANORODS FOR LOW-COVERAGE HIGH-CONDUCTION SYSTEM

Interaction of nanoparticles with biological systems ranging from biomolecules to biological cells is of importance for a range of applications, such as, high-resolution biomedical imaging[50], gene sequencing for molecular diagnostics[51], and sensitive electronic devices[7]. In this Chapter, it will be shown that positively charged cetyltrimethylammonium bromide (CTAB), which is a stabilizing agent used to synthesize different metal nano-shapes[52-55] (such as rods, spheres, cubes, prisms, stars and hexagons), is an effective nanoparticle coating for self-assembling electrically percolating monolayer of different nano-shapes on gram-positive bacterium, such as *bacillus cereus*.

The versatility of CTAB is especially realized for deposition of nanorods, where it is observed that there is four orders of magnitude larger conductivity compared to nanospheres at three times lesser area coverage. For deposition on a "physical surface", the rods do not form electrically percolating channels[56]. Formation of such percolating-conducting network on bacterium is attributed to high adhesion that overcomes steric interaction (responsible for liquid-crystalline order (see Figure 14(b)) leading to random orientation (see Figure15(a)). Furthermore, the strong adhesion (evidenced by conformal deposition of rod causing bending) lowers the contact resistance, leading to 10^4 fold increase in conductivity at 13.5% area coverage compared to spheres with 41% area coverage (see Figure 16). This high conductivity is achieved well below the percolation threshold for random structure at 45% area coverage in two-dimensions[57]. With only ~ 10% of bacterium surface covered, the microorganism may remain alive for longer time

than for > 40% coverage systems with nanosphere deposition[58]. While CTAB alone is toxic to cells CTAB coated nanoparticles are non-toxic[59]. Electronic coupling between nanorod monolayers with microorganisms can open the possibility of novel hybrid devices utilizing the machinery of the biological system.

Bacillus cereus bacteria of size ~ 3-4 μm, with highly negatively charged teichoic acid brushes on its surface, is deposited on silica substrate by the same technique explained in Chapter 3. CTAB coated Au nanospheres and nanorods are prepared in an aqueous solution at pH 4.5 and 6 respectively by a seed-mediated growth process also described below. CTAB forms a bilayer on the nanoparticles and particles are always positively charged independent of pH.

From TEM images the estimated diameters (*D*) for rods and spheres are ~ 25 nm and 45 nm, respectively. The nominal length, l of the rods from FESEM is 400 nm. The nanospheres and nanorods (zeta potential +48 to +71 mV) were deposited by exposing the bacterial substrate to the nanoparticle solutions for only 15 min.

As schematically shown in Figure 14, the nanoparticle deposition is driven by attractive electrostatic interaction between the negatively charged teichoic acid on the bacteria[58] and the positively charged CTAB molecules on the Au nanoparticle surface.

The figure also shows the TEM images of nanorods and nanospheres. Figure 15 shows the resultant morphology indicating three features. Figure 15(a) indicates that nanorods in full contact *bend* under the electrostatic attraction to conform to the bacteria surface. Secondly, primarily at the edges, the rods are partially attached and tend to stick out of the surface. As seen in the inset of Figure 15(a-1), this non-conformal deposition becomes more prevalent at high coverage because the available contiguous space for

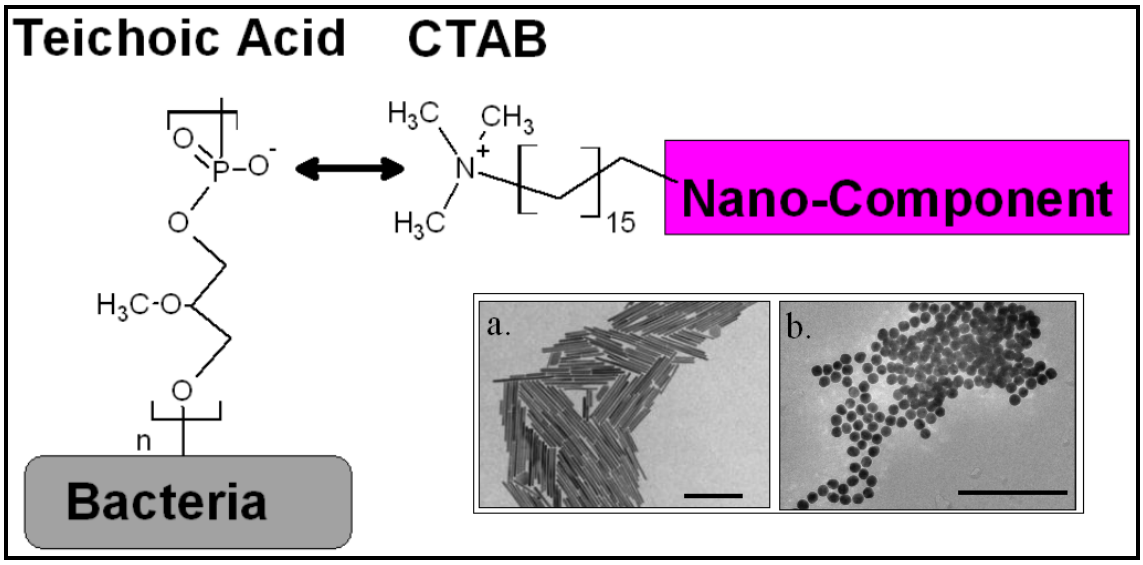

Figure 14. Electrostatic deposition of nanospheres and nanorods is accomplished by capping the nano-component with CTAB that electrostatically binds to the teichoic acid brush on the gram-positive bacterial surface. Insets show the TEM images of (a.) Nanorods and (b.) Nanospheres. Bar size = 500 nm.

deposition is limited and becomes less than the length of the rod making conformal deposition difficult. Thirdly, the deposition of rods on the bacteria is percolating while on the physical surface (see Figure 15(a-2)) it is not. For the conformal deposition where the Au nanorods with modulus 70 GPa[60] bend around the bacteria of a nominal diameter of ~1 μm, the adhesion force due to electrostatic interaction is at least 0.038 N/m or a total force of ~15 nN. The force is comparable to the electrostatic force between positively charged poly-L-Lysine monolayers and negatively charged silica microspheres[61]. If the subtended angle of contact is 2 α along the curvature, the ratio of rod is to microsphere contact area is $\sim 10^{-4}$ for $\alpha \sim 0.05$ rads. Therefore, the force per unit area between nanorods and bacteria is over 1000-fold higher than that between self-assembled monolayers[62].

The current (I) versus applied voltage (V) measurements were made on both nanorod and nanosphere monolayer on bacterial bridges spanning between gold electrodes 7 μm apart. About 3 bacteria make a bridge and a typical device has 10-15 bridges. The measurements showed ohmic behavior as shown in Figure 3. In contrast to poly-L-Lysine coated Au nanoparticle (pH ~ 7) that took 4-8 hours deposition to form a percolating network, CTAB terminated nanoparticles form a percolating monolayer only in 15 min. This is perhaps due to charge compensation of amine groups on Poly-L-Lysine when they are coated on negatively charged nanoparticles. Table in the inset of Figure 16 shows the coverage and conductivity data for the two monolayers.

Analogous to surfactant stabilized conducting polymer in insulating polymer matrix[63,64]; the significantly high conductivity in nanorod monolayer well below the percolation threshold of 45% area coverage for two-dimensional "random" structure[57]; is attributed to the high radius of gyration of the nanorod-cluster due to their random orientation. The high conductivity in nanorods compared to nanospheres as seen in Figure 3-table, could be partly attributed to the fewer number of tunnel junctions in the nanorod network. Assuming random orientation of the rods, the orientation order parameter, $2\langle\cos(\theta)\rangle^2 - 1 = 0$, where θ is the angle between the long axes of the rod and the bacteria. Thus, the average projected length along bacteria axis is $\sim 400/\sqrt{2}$ leading to ~7-fold fewer tunnel junction in the shortest percolating cluster for rods compared to spheres. However this is not sufficient to explain the 4 orders of magnitude larger conductance. We attribute the high conductivity to low contact resistance that could occur due to high rod/bacteria adhesion that presses the rods against each other as they randomly overlay to form the monolayer structure. Furthermore, the contact resistance of

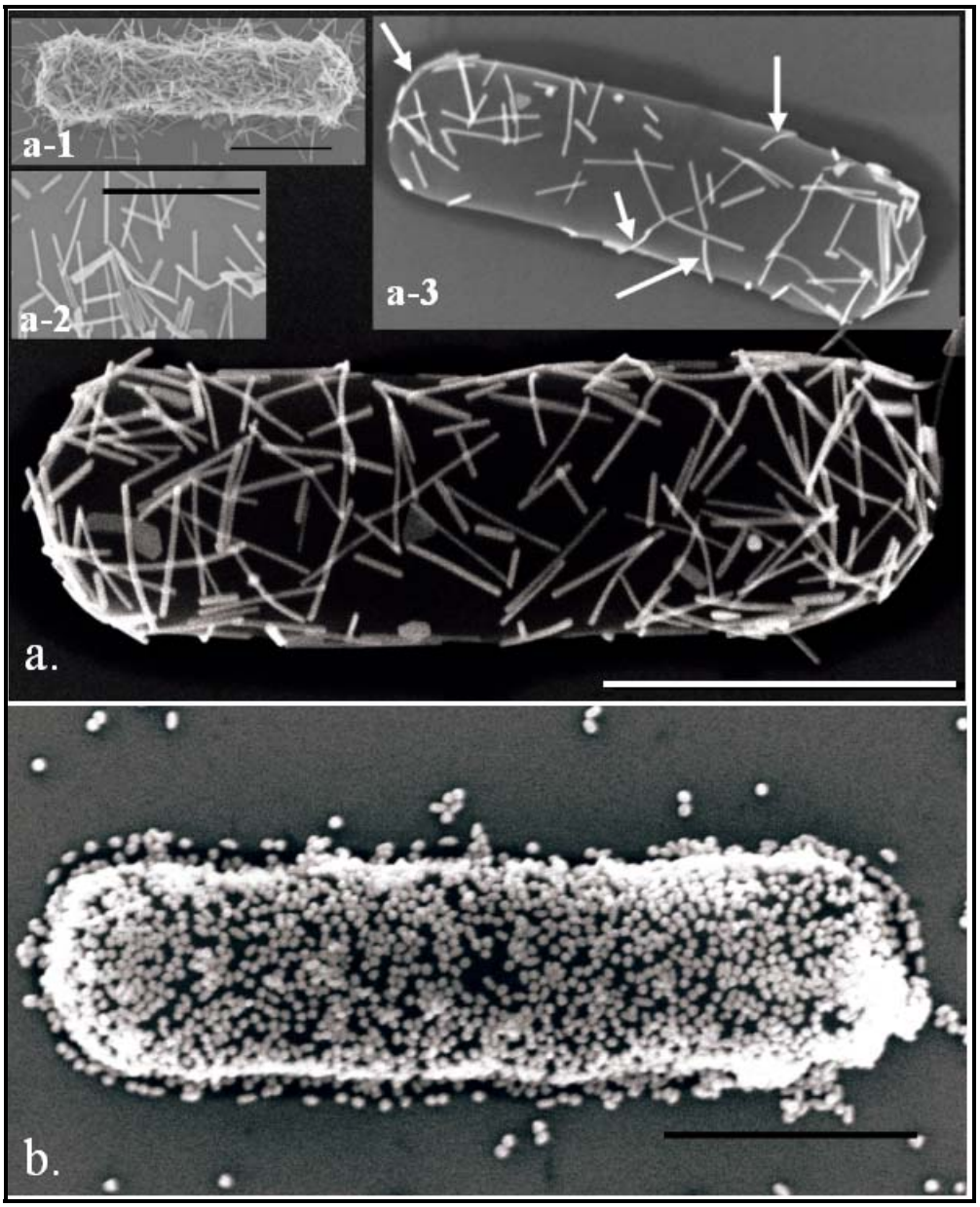

Figure 15. Nanoparticle-deposition on bacteria. (a) Percolating monolayer of nanorods (25 nm in diameter and 400 nm long) is formed in deposition time of 15 min. Nanorods sticking out at the edge of bacteria and conformally deposited on the bacteria can be seen. Inset (a-1) shows deposition on bacteria for 10 hrs. Deposition chemistry is identical to the 15 min. deposition. The inset (a-2) shows deposition of nanorods on a flat silica surface for 10 hrs after sequential monolayer deposition of Poly Allylamine Hydrochloride (PAH) and Poly Sulfonate Styrene (PSS). Inset (a-3) shows low-density nanorod deposition. The arrows indicate bent rods. (b) Nanospheres (45 nm diameter) on bacteria after 15 min. deposition. All the bars are 1μm.

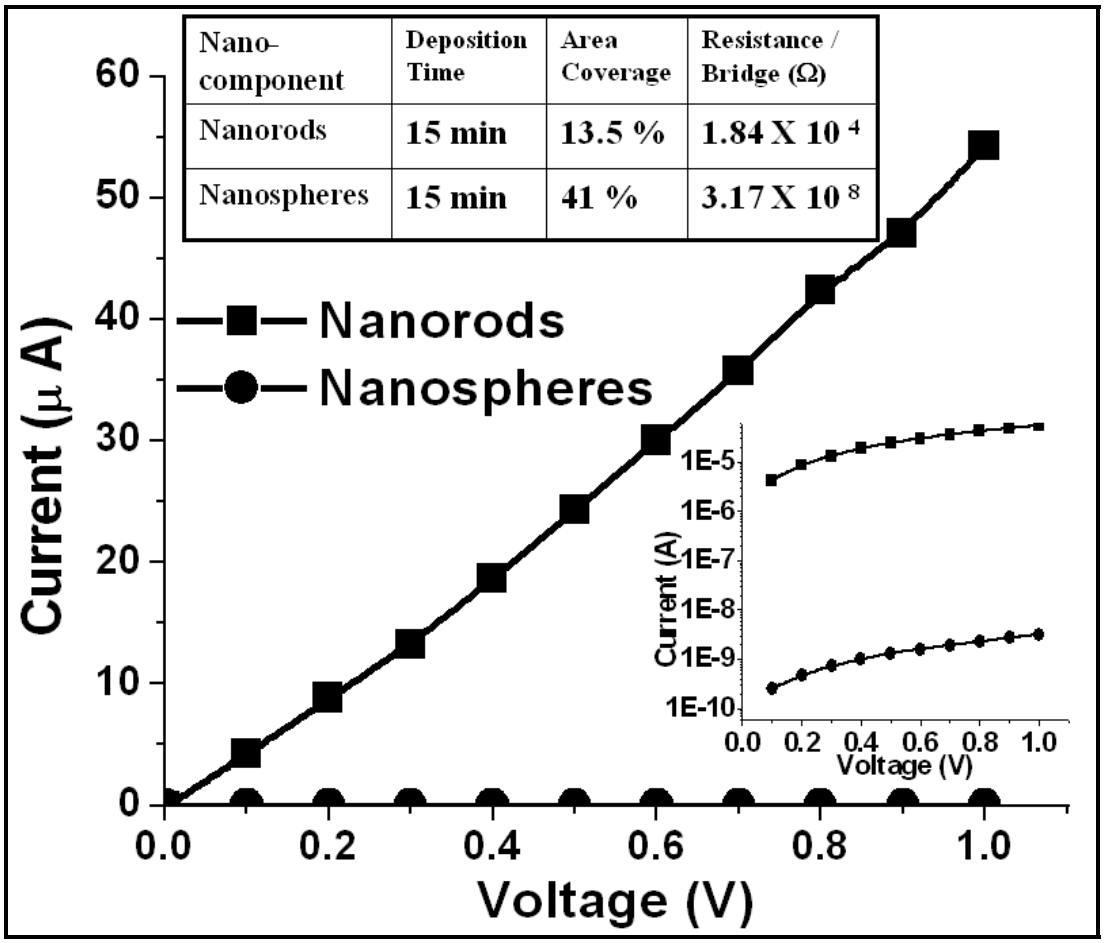

Figure 16. Current (I) versus voltage (V) measurements of nanorod- and nanosphere- monolayer on bacteria. The currents are normalized to single bacteria bridge. The table in the inset shows the corresponding resistance and area coverage of the two nano-components. The process and deposition time is identical to conditions in Figure. 2. The second inset shows log-scale plot of the same I-V characteristics.

the nanorods to the interconnection pads is also lower compared to nanospheres for similar reasons.

Therefore CTAB, which is an effective surfactant to synthesize variety of shapes of nanoparticles, is also an effective capping agent for deposition of nanoscale components on gram-positive bacteria. The strong electrostatic interaction between teichoic acid and

CTAB coating on nanorods results in bending of the nanorods and a four-order enhancement in conductivity compared to nanospheres.

This high conductivity at only ~ 10 % coverage (which is well below the percolation threshold of 45%) opens the possibility of fabricating electronic circuitry on bacteria without suffocating the microorganism.

CTAB-TERMINATED NANOCOMPONENT PREPARATION

Nanorod Preparation

Synthesis of gold nanoparticle seeds.

Gold seeds were synthesized by a previously described method[65]. Specifically, to a 10 ml 0.1 M aqueous solution of CTAB was added 250 µl of 0.01M $HAuCl_4$ and kept under stirring conditions. To this stirred solution was added 0.60 ml of 0.01 M sodium borohydride, which resulted in the formation of a brown-yellow solution. Vigorous stirring of this seed solution, which was kept at 25 °C, was continued for 2 min. This seed solution was further used for the synthesis of gold nanorods after 30 min of its synthesis. The size of these seed particles was less than 4 nm.

Synthesis of gold nanorods by seed mediated approach[66].

Gold nanorods were synthesized by the three-step seeding protocol as described previously[67]. Specifically, two 20 ml conical flasks and one 100 ml conical flask (labeled A, B, and C, respectively) were taken. To these flasks were added 9 ml (in flasks A and B) and 45 ml (in flask C) of growth solution containing a mixture of 2.5×10^{-4} M $HAuCl_4$ and 0.1 M CTAB solution. To these solutions were added 50 µl (flasks A and B) and 250 µl (flask C) of 0.1 M freshly prepared ascorbic acid, and the resulting solutions were

stirred gently. The orange color of the gold salt in the CTAB solution disappeared when ascorbic acid was added. We have attributed this color change to the reduction of Au^{3+} to Au^{+}. However, the reduction of Au^{+} to Au^{0} does not occur, and we do not observe the gold plasmon band indicative of Au^{0} nanoparticles even after 24 h. This indicates that ascorbic acid is too weak to reduce Au^{+} under our experimental conditions. However, further reduction of Au^{+} to Au^{0} occurs when 1.0 ml of the seed solution is mixed with sample A (step 1). This is evidenced by a rapid development of red color to the solution in sample A, which earlier was colorless, thus indicating the formation of gold nanoparticles. After 15 s, 1.0 ml of sample A was mixed with sample B (step 2). This leads to a color change in sample B, indicating the generation of gold nanoparticles. The reduction in this case is slower compared to that in step 1. A 5.0 ml portion of sample B was further added to sample C after 30 s (step 3). The color of this solution slowly changed to purple. In all cases, each flask was gently stirred to homogenize the solutions. The solution in flask C was kept at 25 °C for a period of 16 h. After the solution was stored for 16 h, purification was necessary to obtain gold nanorods. All the top red-brown solution (which contains mostly spheres) was slowly removed by suction. A faint brown tinge can be observed at the bottom of the flask. A 5.0 ml sample of deionized water was flushed into the beaker, and the contents were agitated for some time. A greenish-brown color developed in the deionized water and intensified upon repeated agitation. This solution contains a high percentage of gold nanorods, though other shapes (triangles, hexagons, and small rods) are also present in small amounts. The excess CTAB was removed by centrifugation twice (at 7000 rpm) and washing with deionized water.

Characterization:

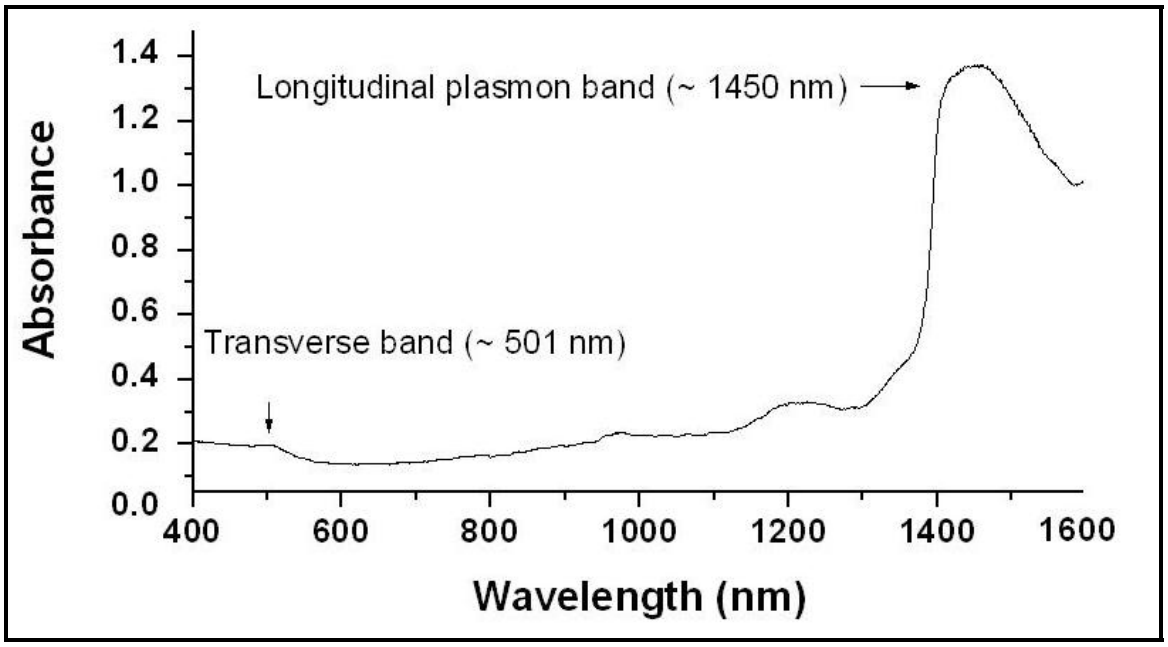

Figure 17. UV-Vis spectra of gold nanorods in D_2O. It shows the traverse (501 nm) and longitudinal (1450 nm) plasmon band for nanorods.

The UV-vis measurements were carried out by dispersing the nanorod solution in D_2O. The transverse (~ 500 nm) and longitudinal plasmon band (~ 1450 nm) can be clearly seen in the figure.

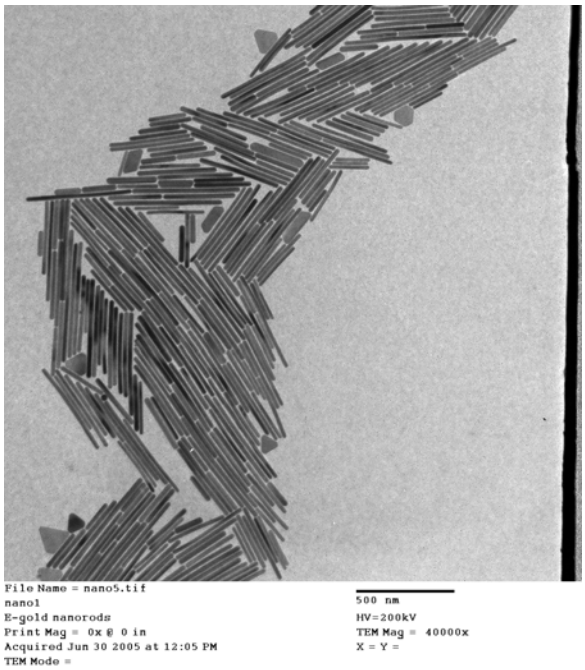

Figure 18. TEM image showing CTAB terminated nanorods of size ~ 400 nm length and thickness ~ 25-30 nm.

Nanosphere Preparation[68]

For the preparation of large size gold nanospheres, gold nanoparticle seeds are prepared by reducing 1 ml of 10 mM $HAuCl_4$ with 1 ml of 100 mM $NaBH_4$ in the presence of 1 ml of 10 mM sodium citrate and 36 ml of fresh deionized water (DI) water. The resulting mixture is aged for 2-4 hours in order to allow the hydrolysis of unreacted $NaBH_4$. These gold nanoparticle seeds exhibit a plasmon resonance peak at 500 nm, and have an average diameter of 5.2 ± 0.6 nm.

Three growth solutions are then prepared for seed-mediated growth step. The first two solutions (1 and 2) contained 0.25 ml of 10 mM $HAuCl_4$, 0.05 mL of 100 mM NaOH, 0.05 ml of 100 mM ascorbic acid, and 9 ml of a 7.5 x 10^{-2} M CTAB solution. The third solution (3), contained 2.5 ml of 10 mM $HAuCl_4$, 0.50 ml of 100 mM NaOH, 0.50

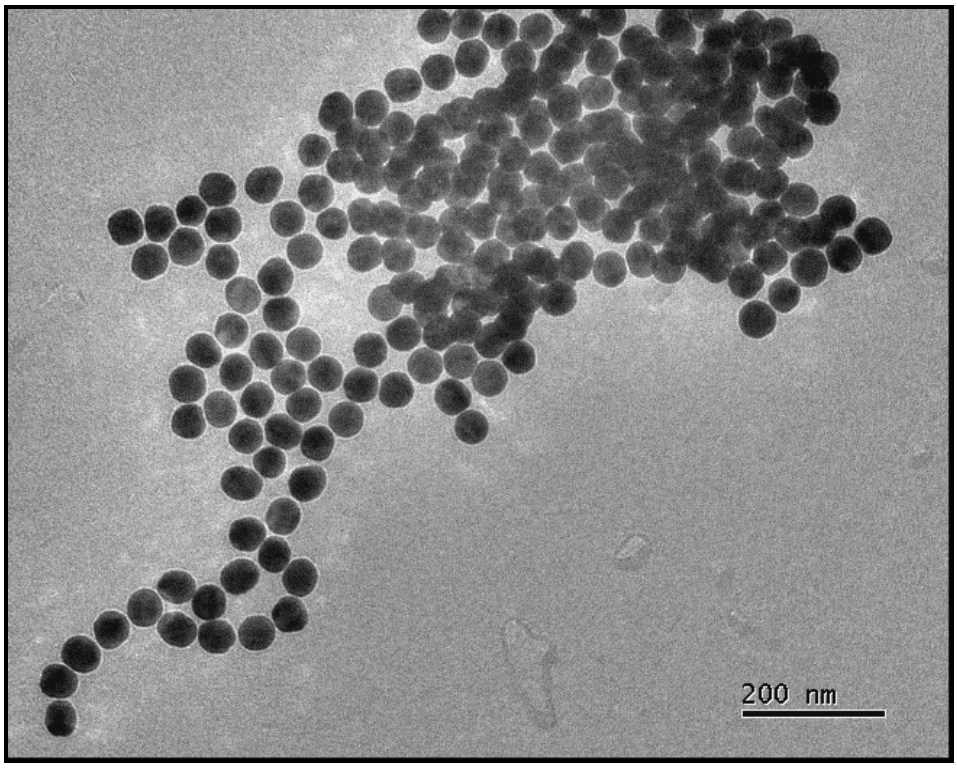

Figure 19. TEM image showing CTAB terminated nanospheres of size ~ 40-45 nm.

ml of 100 mM ascorbic acid, and 9 ml of CTAB solution.

Nanosphere formation with large diameter was initiated by adding 1 ml of seed solution to growth solution 1. After 5 mins, one ml of resultant solution 1 was then added to 2, and then again after 5 min all of the resulting growth solution in 2 was added to 3. After the addition, the color of 3 changed from clear to deep magenta-purple over a period of 30 minutes.

Solution exhibited a plasmon resonance peak at 535-540 nm, and had nanospheres with average diameter of 40-45 nm. This solution is then centrifuged at 8000 rpm for 20 mins to remove the excess CTAB and the precipitated gold nanospheres is redispersed in DI water.

EDAX and FTIR studies and the zeta potential measurements revealed that surfactant CTAB molecules, adsorb onto surfaces of the gold nanocrystals and play major roles in the direction-specific self-assembly of the coated nanocrystals via inter-digitation of the tails forming a bilayer. The cationic head groups face the solvent. The interparticle spacings were similar irrespective of the size and shape of the gold nanocrystals. The zeta potential of the nanorod and nanospheres are in the range of +48 mV to +71 mV, which suggests that they are positively charged. The deposition on nanorods on positively charged physical surface showed no deposition and on negatively charged surface showed deposition, indicating that the deposition is electrostatic[69].

7. POLELECTROLYTE – NANOPARTICLE HYBRID SYSTEM

Electronic/mechanical nano- & molecular devices have attracted a lot of interest recently. Such devices have shown electronic effects like negative differential resistance[70], and molecular switches[71,72] or mechanical effects like molecular motors[73,74]. All these devices are based on complex molecules, which have specific characteristics which when combined with external stimuli, behave in a way that could be captured as change in either their electrical or mechanical response. Such nano-electronic devices have the potential of achieving high performance complex functions with significantly low power consumption. Last decade has seen great applications of polyelectrolytes like Poly alylhydrochloride (PAH) and Poly Styrene Sulfonate (PSS) for self-assembly as a monolayer to deposit nanoparticles on various substrates. The deposition of nanoparticles in single step is although not percolating for such systems and thus far the polyelectrolyte deposition has only been monolayer in nature and on plain surface of macroscopic sizes.

The last few Chapters have shown that the bacterial surface acts as a very effective scaffold to deposit nanoparticles because it has polyelectrolyte brushes on it. These brushes shield the charge on the nanoparticles. In this Chapter it will be shown that polyelectrolyte PAH fiber can also be used as an effective scaffold to selectively deposit percolation layer of gold nanoparticles (with an average tunneling distance of 0.168 nm, which is comparable to the PAH thickness of 0.162 nm) in a single step, without breaking or loosening the PAH fiber and use its high hygroscopic nature to build a highly sensitive, ultra-fast humidity sensor. Here a very simple process of using heat annealing

of PAH fibers to attach them strongly to silica substrate will be shown. On these nanoparticles or other charged physical or biological species could be deposited to make complex hybrid structures and devices.

Silica substrate having gold electrodes placed 7 μm apart are oxygen-plasma-treated to clean the chip and introduce hydroxyl groups. The chip is then washed with n-octadecyltrichloro silane, a hydrophobic silane, for 2 hrs to deposit a monolayer of the silane to make the silica surface hydrophobic. The chip is then washed with 1% dodecylethiol solution overnight, which deposits as a monolayer on the gold surface to make it hydrophobic too. A 40% solution of positively charged polyelectrolyte poly-allyl hydrochloride (PAH) solution is then spun to make micro-fibers, which are placed across the electrodes on the hydrophobic silica-gold chip prepared earlier. Nano-fibers could also be deposited on the chip by electrospinning, although the electronic properties show no conduction. Once the PAH micro-fibers are laid between the electrodes, the chip is baked in the presence of atmospheric oxygen for 6 hrs. This is assumed to make the fiber base stick to the silica surface. If the chip is not baked, the PAH fiber washes away with a simple water wash. Also if the unbaked chip with fiber is simply kept out for 2 days, the PAH fiber dewets and forms chain of beads. After baking, the chip is washed with de-ionized water to get rid of excess PAH, which is loosely bound to the fiber. This excess PAH does not deposit elsewhere on the chip since all the other surfaces are neutral and hydrophobic. The rest of the PAH is assumed to be held to each other via inter-twining or cross-linking, and the fiber does not peel off. After baking, the chip is put in negatively charged gold nanoparticle solution. The nanoparticles deposit on the chip in 8 hrs forming an electrically percolating array as shown in Figure 20. As can be seen (Figure

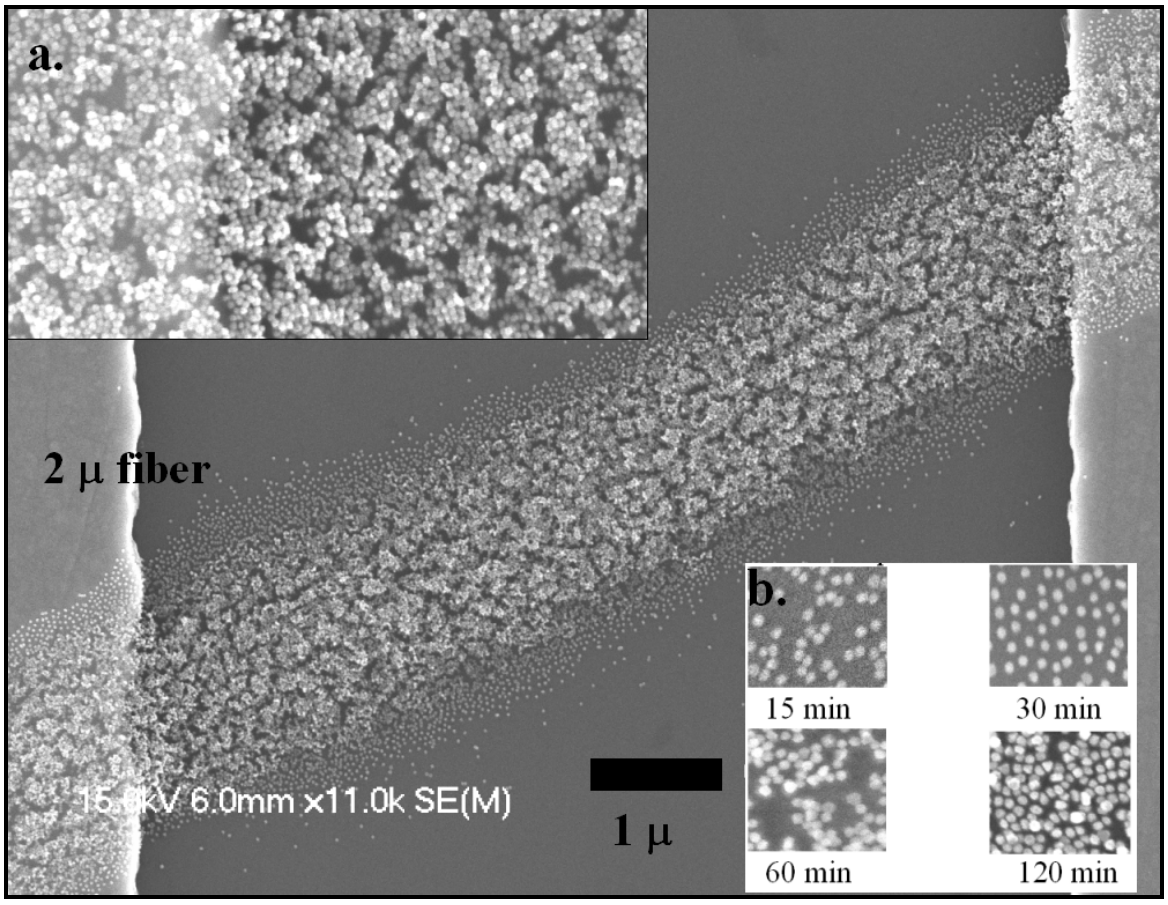

Figure 20: SEM image showing 30 nm gold particles deposited on PAH fiber 2 μm in diameter deposited across 7 μm wide gold electrode pads. Bar size = 1 μm (a.) High magnification SEM images of nanoparticles deposited on PAH fiber. The image shows that the deposition is percolating and the density is same on the gold pad and silica. (b.) Deposition density of nanoparticles on the center of the fiber after 15 mins, 30 mins, 60 mins and 120 mins.

20a.), there is a multilayer deposition of nanoparticles, which implies that the nanoparticles diffuse into the fiber while depositing. The deposition density after 8 hrs is ~1000 nanoparticles/μm^2, which would have covered 90% of the area had the deposition been a monolayer, as against only 76% in this case. The negatively charged nanoparticles are also assumed to cross-link the PAH on the fiber making the device more stable. The inset of the figure (Figure 20b.) shows the deposition rate at the center of the 2 μm fiber. As the deposition time in increased from 15 min to 2 hrs, it can be seen that the

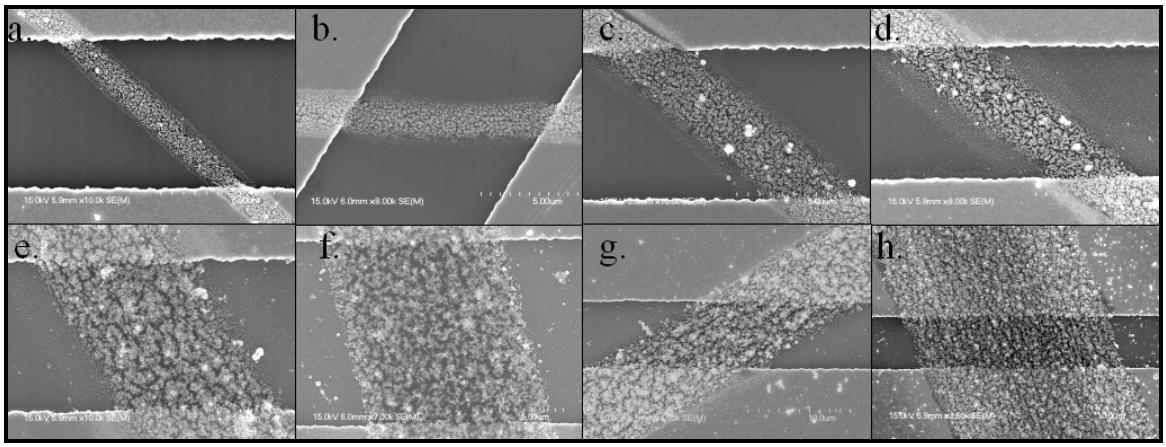

Figure 21. Various fiber devices of different sizes. (a) 1 μm (b) 2 μm (c) 4 μm (a) 5 μm (a) 6 μm (a) 7 μm (a) 8 μm (a) 22 μm. This illustration shows that various sized fiber devices can be built using this technique.

deposition density goes from monolayer to multilayer. From the figure, somewhere between 30 minutes and 60 minutes of deposition, the nanoparticles start diffusing inside the fiber. After 8 hrs, the deposition is highly conductive. The nanoparticles can be deposited on fibers of size 1.5 micron to 25 micron as shown in the figure 21. Interestingly the deposition of the nanoparticles occurs in clustered domains,which is probably because of the cross-linking action of the nanoparticles as can be seen from the high magnification SEM image of the fiber (Figure 20a.). The conductivity (IV) and the humidity sensor application of the device will be discussed in the next Chapter.

8. HUMIDITY SENSOR ON POLY-ELECTROLYTE FIBER

The conductivity of the device can change by 2 orders of magnitude when the humidity is changed from 21% to 1.5% rH, which makes this the most sensitive humidity sensor for low humidity measurements. This robust and reversible change occurs because of the change in the dielectric tunneling barrier and is ultra-fast with about 3 ms response time, as measured from sound-wave instigated change in the atmospheric humidity. Simple conductivity study shows that the PAH fiber-nanoparticle device shows near ohmic conductivity (Figure 22a.). The voltage is applied to the device from 0 V to 3 V with a step size of 100 mV, on a device with 25 μ fiber at two humidity values (1.5% and 21%, discussed later) and current is measured. It is observed that there is a two order of magnitude difference in current between 21% and 1.5% humidity. The I-V curve shows a slight curvature. This curvature is probably due to coulomb blockade where the electron transport from one nanoparticle to another experiences repulsion from an electron-charged nanoparticle. As the current increase, the resident time of electron in the nanoparticle reduces leading to lesser and lesser blockade, and more and more conductivity. This effect can be seen from the differential conductivity of system shown in the inset (Figure 22 a.2). Also, the shape of the curve does not change with humidity as can be seen from the logarithm curve (Figure 22 a.1). Next the effect of temperature is studied on the device conductance. When the device is brought down to a temperature of 5 K, the device undergoes a slight drop in the current as shown in Figure 22 b. This drop in electronic flow (current) follows the Arrhenius law with the activation energy of

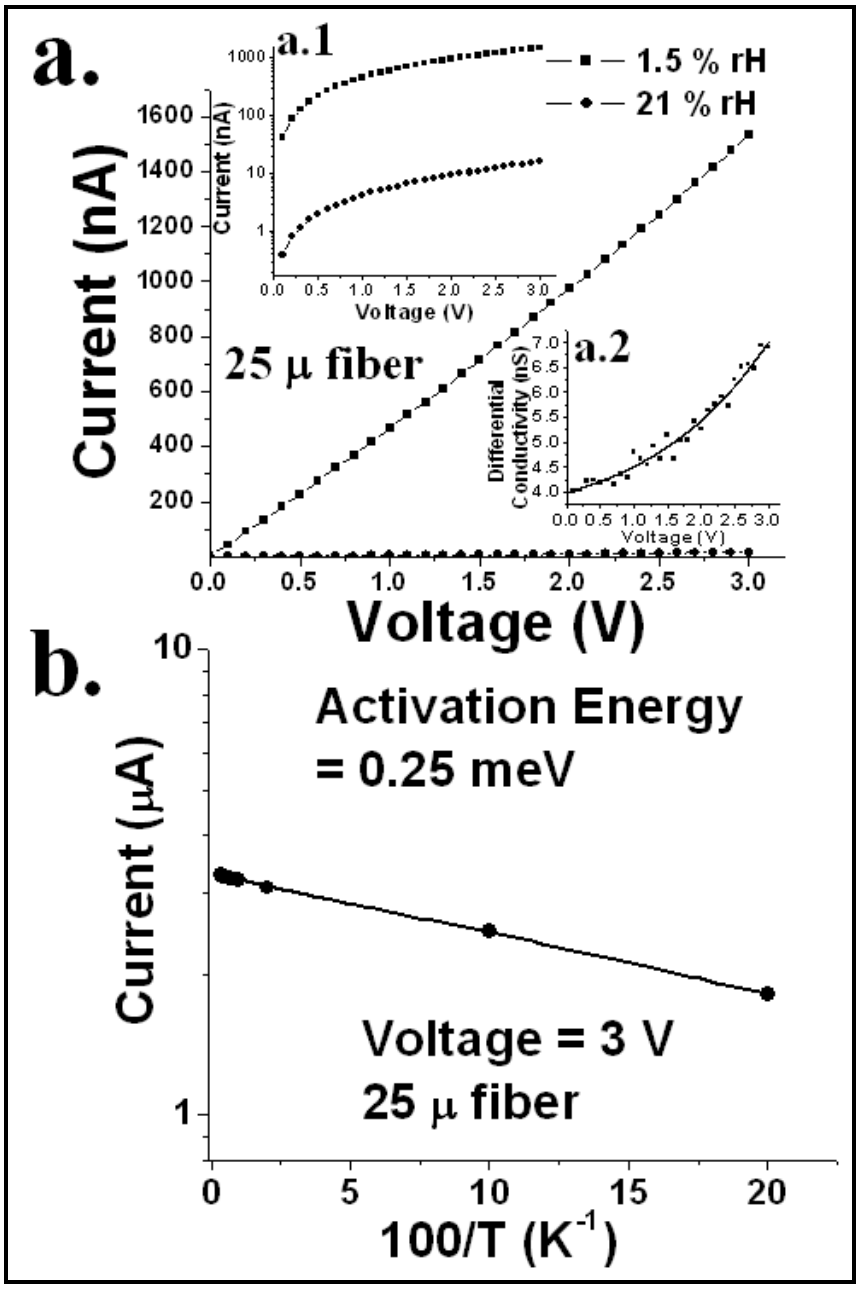

Figure 22: (a.) Current Voltage (I-V) behavior of a 25 μm fiber device, where voltage is increased from 0 to 3 volts with a step size of 100 mV. The IV are shown at two humidity values (1.5% and 21% rH). Notice the small curvature in the curve. (a.1) Log chart of I-V showing that the I-V behavior at the two humidity values is similar. (a.2) Differential conductivity of the device in nS, showing an increase in differential conductivity with voltage, indicating nanoparticle's coulomb blockade effect. (b) Current (I) Versus temperature (100/T) data at 3 V bias for a 25 μm fiber device. Activation energy for electron transport of 0.25 meV indicates electron transport is through electron tunneling.

electron tunneling of 0.25 meV, 100 times lower than kT at room temperature. This small activation energy implies that the electron transport is through electron tunneling mechanism. Next we will discuss the device's response to humidity change.

The device shows a remarkable change in conductivity with humidity as shown in the IV, for 25-μ fiber-device were there is an increase in conductivity by 2 orders of magnitude from 20% to 1.5% humidity. Since PAH has a high hygroscopicity, the change in humidity leads to a drop in the water content of the fiber. This decrease in the water content leads to a decrease in the dielectric constant of the media through which electrons tunnel. Electron tunneling being the electron transport mechanism, this decrease leads to an increase in the currents as seen in the Figure 23. At 1 volts, the device with 7 μ fiber shows an increase in conductivity by ~ 50 folds (25 μ by ~ 100 folds) as the humidity goes from 40% to 1.5% relative humidity. The figure also shows the robustness of the device, as it has no hysteresis when the humidity is brought back to 40%. The inset of the Figure (Figure 23a.), shows the actual current values. The other inset (Figure 23b.) shows the device made of 7 μm fiber laid across 7 μm gold electrodes, with fiber having nanoparticles deposited for 8 hrs.

As the humidity changes, the amount of water absorbed by the fiber also change following the Henry's law and the water content in the fiber is given by fH, where f is the Henry's constant and H is the humidity of the surrounding. Assuming the dielectric of the tunneling junction follows a linear average extrapolation of the dielectric constants of PAH and water components, the dielectric constant of the junction at a given humidity is given by (fH/100) X 80 + (1 – (fH/100)) X 3 = 0.77 fH + 3. Using this value of dielectric

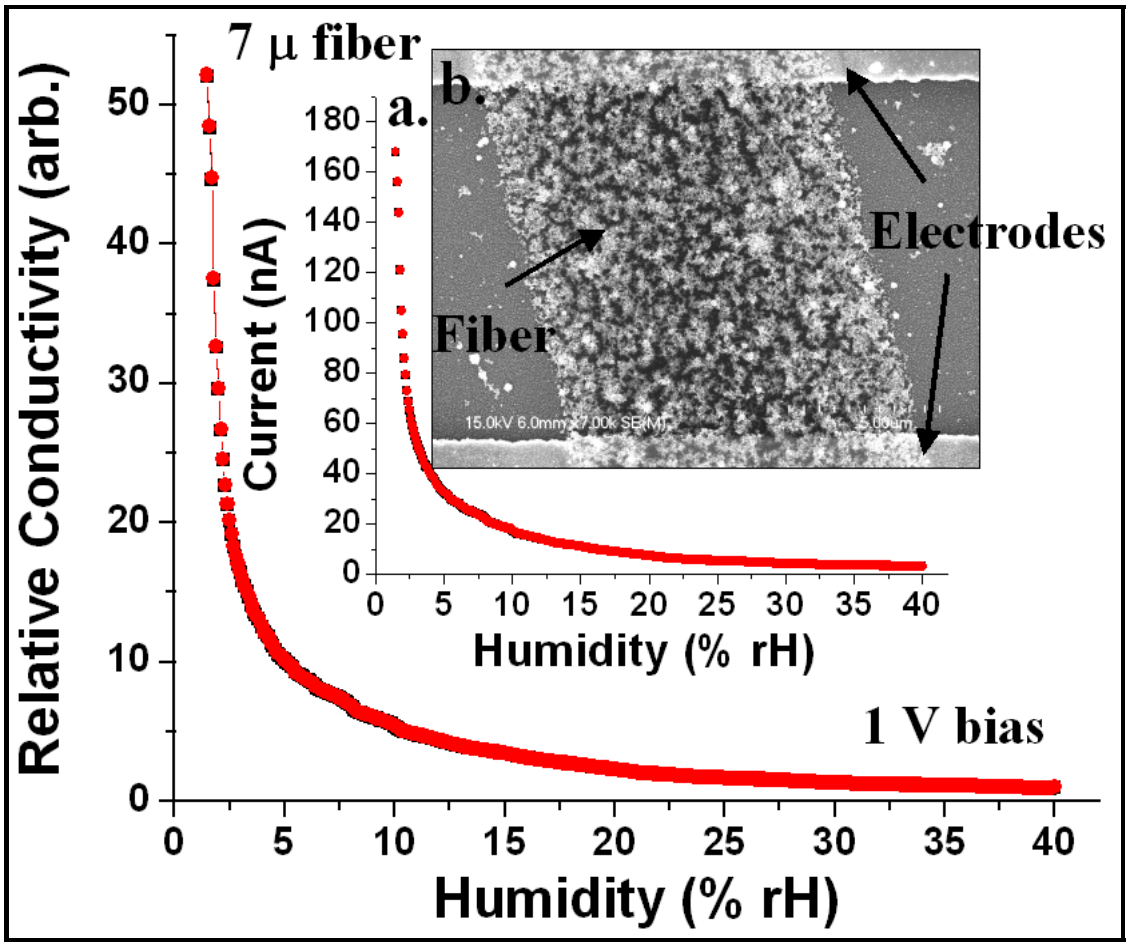

Figure 23: Relative conductivity of the device versus humidity at 1 V bias for a 7 μm fiber. The figure shows that there is no hysterisis when the humidity is brought back to 40% rH. (a.) Inset shows the value of the current for the device at 1 V applied bias. (b.) Inset shows SEM image of the 7 μm fiber spanning across the electrodes.

constant and Fowler Nordheim equation for electron tunneling, a model for the electric current through the system was derived (Equation 1). Notice that the electron tunneling also changes with the change in the electron tunneling distance. But when the parameter was put in the fit, it showed no change with humidity. This is expected since the nanoparticles crosslink the polymer network and so they cannot move relative to each

other. The Fowler-Nordheim equation for electron tunneling showing the change in conductance of the system with humidity is given below.

$$I = \left\{ C \exp\left[-Ka\left(1 - \frac{A}{\sqrt{(0.77H + 3)}} \right)^{1/2} \right] \right\}$$

Here, I is the measured current, *a* is the average electron tunneling distance between the nanoparticles and Ro, K, and A are constants. K and A are given below.

$$K = \frac{2(2m_e)^{1/2}\phi^{1/2}}{\hbar}$$

$$A = \frac{1}{f}\left(\frac{e^3 E}{4\pi\varepsilon_0 \phi^2} \right)^{1/2}$$

Here, m_e is the mass of electron, ϕ is the work function of gold, e is the charge on electron, $\hbar$ is the Planck's constant and E is the electric field between the nanoparticles.

Figure 24 shows the fit of the Fowler Nordheim equation (Equation 1) for fibers of size 1, 2, and 7 μm, where relative conductivity at 2 V bias is shown to change with the change in humidity from 1.5% to 21%. All the fits have a coefficient of correlation of > 0.985. The change in the conductivity for 1, 2, and 7 μm fibers is ~ 7.1, 14.1 and 30.8. The inset in the figure shows a table with the fitting parameters. It can be seen that the parameter A does not change much over the three sizes. Using the value of K from the above equation, the average distance between the nanoparticles, is calculated to be 0.183 nm, which close

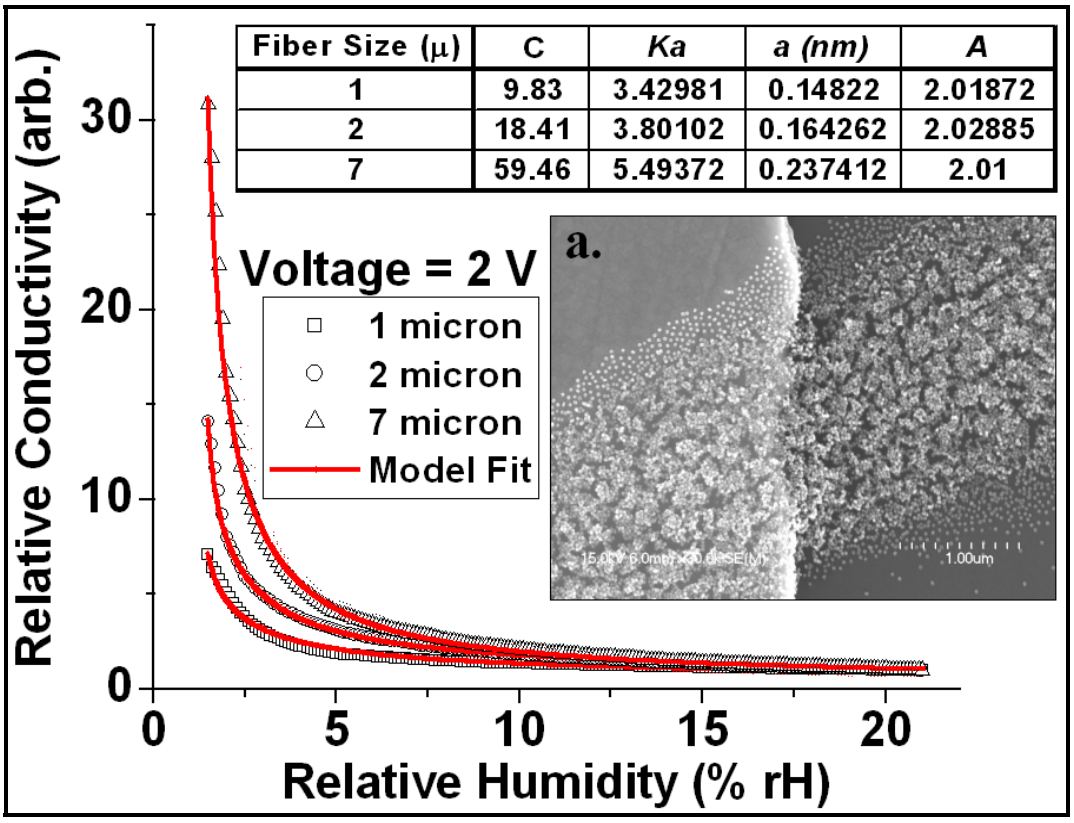

Figure 24: Relative conductivity versus humidity data and model fit for 1, 2, and 7 μm fiber devices at 2 V bias. The dark line shows the model fit. It can be seen that the model fits the data very well. The inset-table shows the values of the model parameters. (a.) High magnification SEM image showing good contact of the fiber with gold electrode.

to the thickness of the PAH molecule of 0.162 nm, suggesting that on an average there is a single monolayer of PAH between the nanoparticles taking part in the electronic conduction. This also shows that the nanoparticles cross-link the PAH network together. The parameter C should be proportional to the number of conducting channels through which the electrons tunnel. The parameter C is reasonably linear to the fiber size showing that the nanoparticle network on each fiber is similar. The slight increase in *a* with the fiber size, could be because of averaging over more number of routes for electron

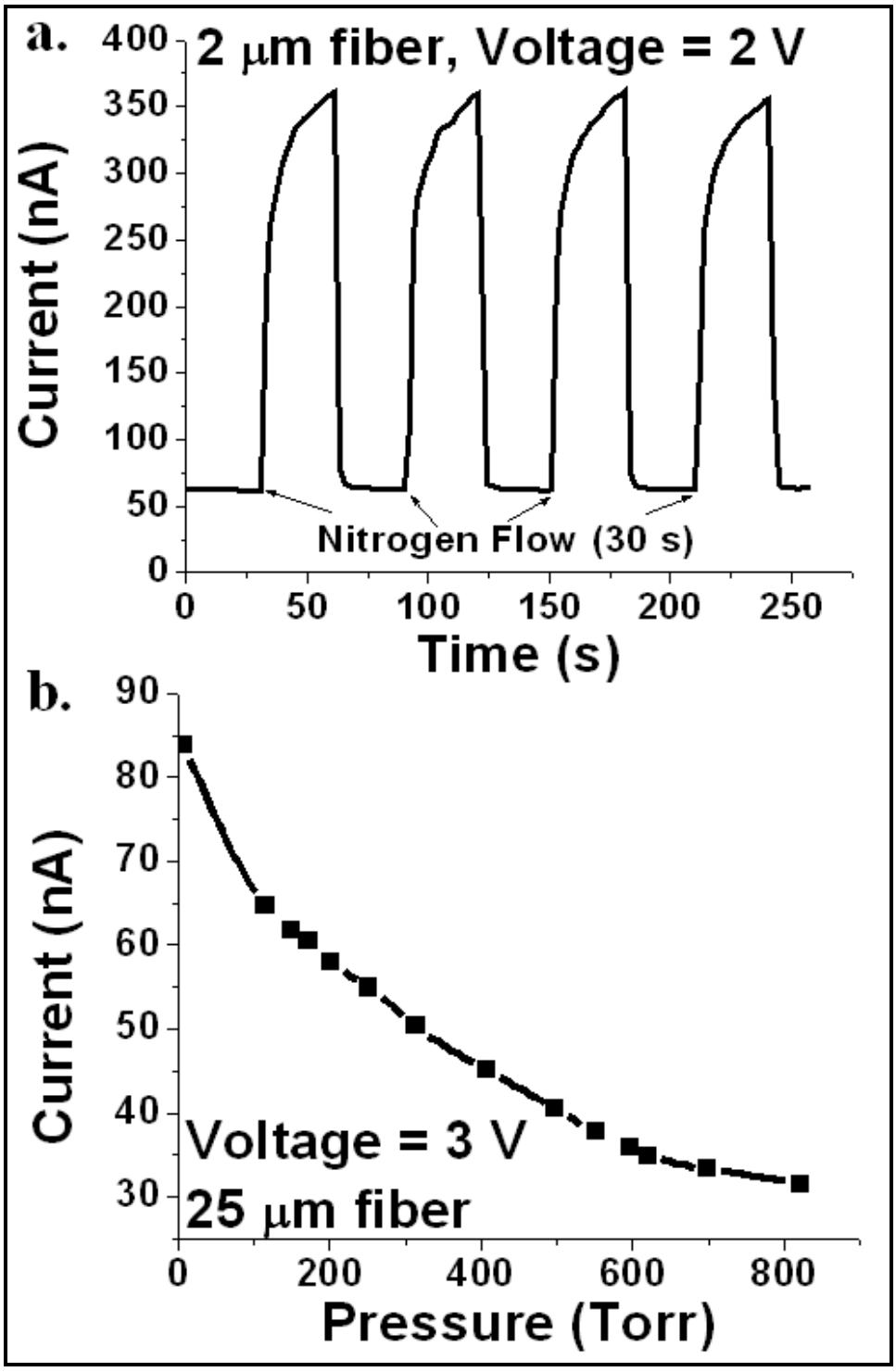

Figure 25: (a.) Multiple times exposure of dry N_2 gas (30s exposure time) over a 2 μm fiber device shows the robustness of the device. The current values at 2 V bias drop fast when the N_2 is turned off showing a quick response time. (b.) Change in conductivity with pressure for a 25 μm fiber device at 3 V bias.

tunneling. This would make the larger diameter fibers more sensitive to humidity than smaller ones. This can be seen in comparison with Figure 22a, where the change in conductivity for 25 μm fiber is ~ 90 folds, while for the 1 μm is only 7 folds, for a humidity change from 21% to 1.5%. Also interesting to see here is the fact that there is no leakage current in this system as against the humidity sensor device made on bacteria[58]. The high magnification SEM image in the inset (Figure 24a.) shows that there is good contact of the nanoparticles on the device with gold electrode.

When dry nitrogen is flown over the device, the humidity reduces and the currents increase, and when the nitrogen flow is switched off, the currents come back to the same value. Repeated flow of dry nitrogen gives the same results and indicates that the device is highly robust as shown in Figure 25a. In this experiment, a 2 μm fiber device at room humidity of 38% rH is subjected to a 2 V bias and is exposed to dry nitrogen for 30s intervals and the current is measured. As can be seen from the figure, when the nitrogen flow is stopped the current drops immediately. This shows that the device has a very fast response. To study the response further, we installed a high power speaker in front of the device as shown in Figure 26. Then by using a 1 mm I.D. diameter pipe, flowed nitrogen through the device at 1 cm^3/s such that it mixes with some air and the humidity is low but not zero. This brings the device in the high sensitivity (to humidity) region. The speaker produces sound at various frequencies from 100 Hz to 1000 Hz. These sound waves, which are essentially pressure waves, produce sinusoidal pressure changes. This translates into sinusoidal change in the humidity around the device as shown in the equation below (Table 1). This in turn leads to change in current at the frequency of sound. A lock-in amplifier attached to the system measures the current at the sound

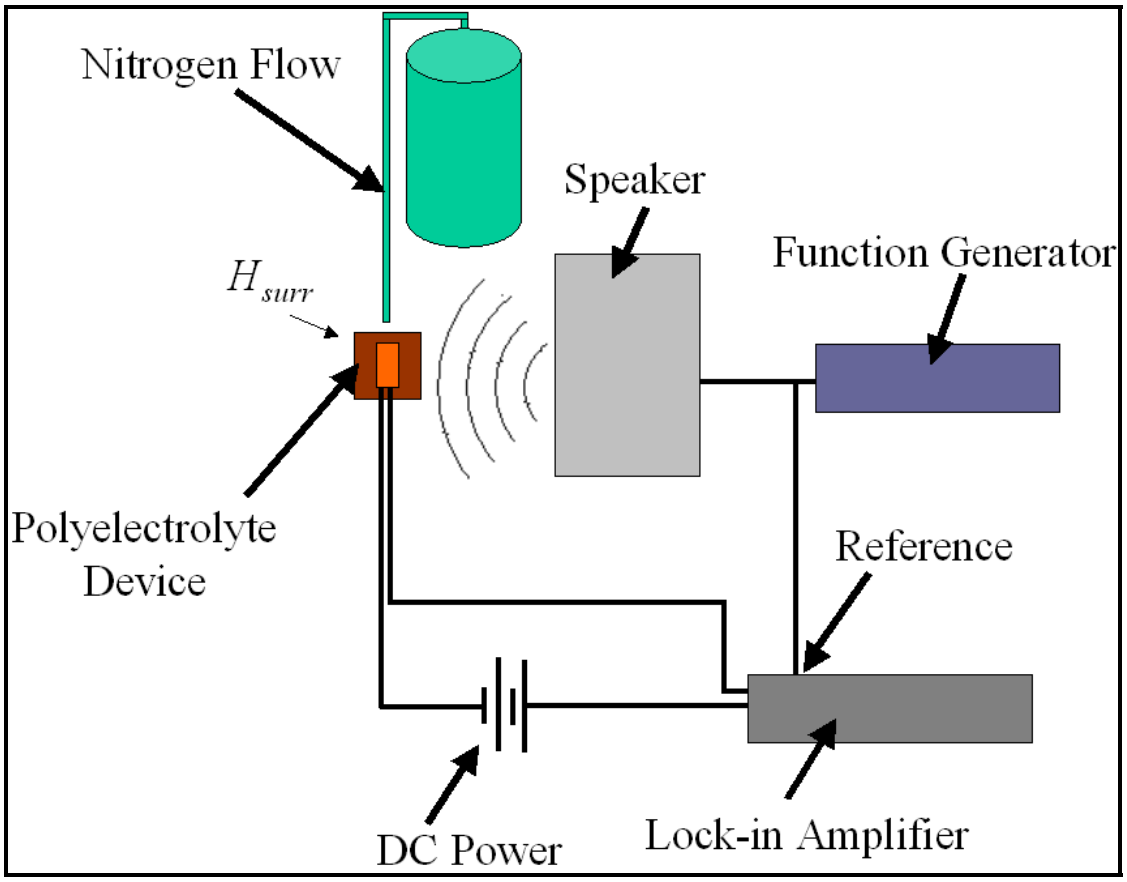

Figure 26: Sound wave experimental Setup. Device attached to a DC source with nitrogen flowing through it and the current is input to a lock-in amplifier. The sound waves change the current through the device with the frequency of the sound wave which is picked-up by the lock-in amplifier set at the same reference frequency.

frequency. For a 25 μ fiber device, with a total current of 15.5 μA at 1 V in dry nitrogen atmosphere, for sound frequency from 100 Hz to 330 Hz, the AC current remains almost constant at 3.1 μA (rms) as measured by the lock-in amplifier. The water goes through three steps during its interaction with sound; it diffuses to the surface of the fiber, it adsorbs on the fiber and then it desorbs again and again, producing the sinusoidal change in conductivity. It is assumed that probably diffusion and adsorption/desorption goes to completion and reaches steady state in the time scales of these frequencies and therefore

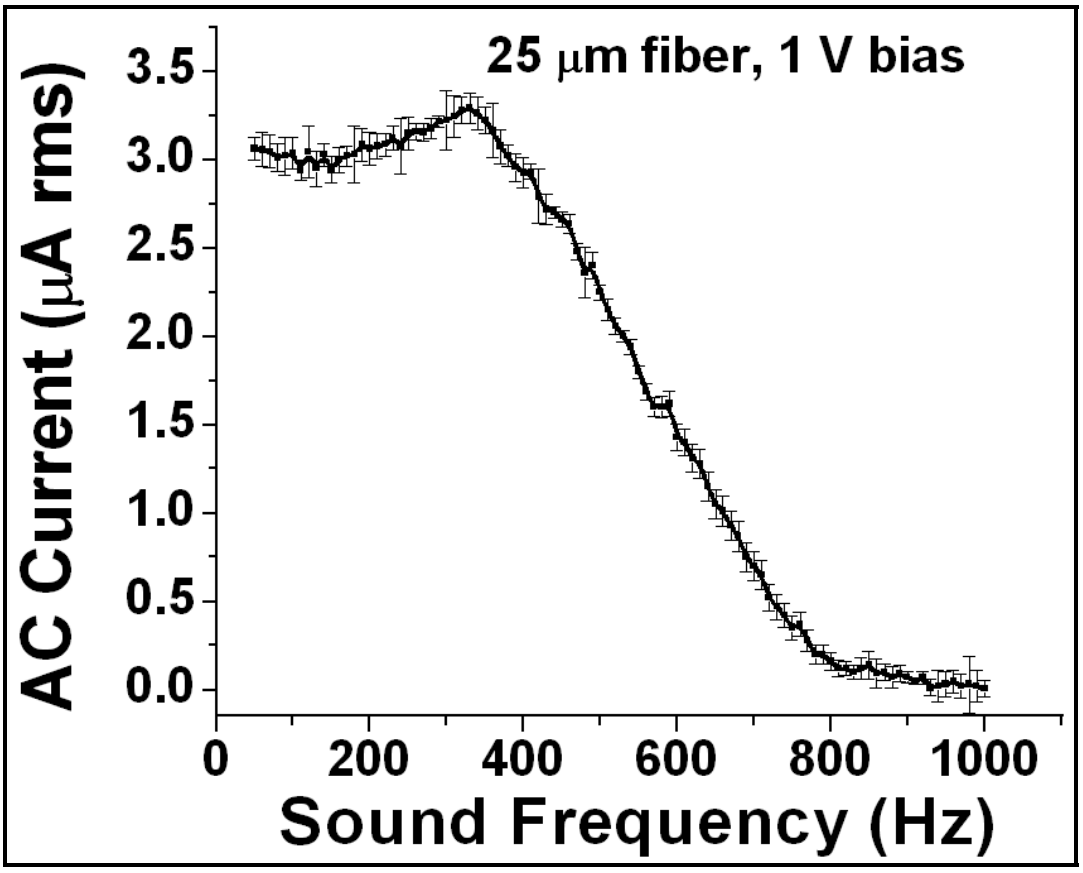

Figure 27. Change in AC current response of the device with change in sound frequency, which displaces nitrogen flowing on the device. The fiber size is 25 mm and the voltage applied is 1 V. The maximum AC rms possible from DC measurements is ~ 3.1 μA, which comes at 330 Hz.

these are not the rate-limiting step (equation in Table 1). This means that in the time scale of these frequencies the complete mass transport of water takes place. Solving the equation in this region shows that the amplitude of humidity should not change with frequency. After 330 Hz the amplitude of the AC current starts decreasing. This is expected since may be in these time scales the mass transport from diffusion and adsorption/desorption is not complete and the processes are in unsteady state. These effects can be seen in the diffusion equation in Table 1. It can be seen that the humidity

Mass transport at steady state	Diffusion at unsteady state
$H = \frac{P_w}{P_s}$ $P_w = yP$ $P = P_{atm} + P_o \sin(\kappa x + \omega t)$ $H = \frac{yP_{atm}}{P_s} + \frac{yP_o}{P_s}\sin(\kappa x + \omega t)$ $H = H_{surr} + \frac{yP_o}{P_s}\sin(\kappa x + \omega t)$	$J_{H_2O} = -D_{H_2O}\frac{\partial}{\partial x}(c) = -\frac{D_{H_2O}y}{RT}\frac{\partial}{\partial x}(P)$ $\frac{\partial}{\partial t}N_{H_2O} = -\frac{D_{H_2O}y}{RT}\frac{\partial}{\partial x}\left(P_o \sin(\kappa x + \omega t)\right)$ $\frac{\partial}{\partial t}N_{H_2O} = -\frac{D_{H_2O}y\kappa P_o}{RT}\cos(\kappa x + \omega t)$ $N_{H_2O} = \frac{D_{H_2O}y\kappa P_o}{\omega RT}\sin(\kappa x + \omega t)$ $H = H_{atm} + KN_{H_2O}$ $H = H_{surr} + \frac{H_o}{\omega}\sin(\kappa x + \omega t)$

Table 1: Equations for change in humidity and water content of the device with sound waves. The two cases here are 1) steady state and, 2) diffusion with unsteady state. *y* is the mole fraction of the water vapor, ω is the frequency of sound, *P* is the total pressure, P_{atm} is the atmospheric pressure, P_o is the amplitude of the sound wave, P_s is the saturation pressure, and H_{surr} is the average humidity around the device.

response is inversely proportional to frequency. This will lead to inverse proportionality of AC conductivity as well as can be seen in the figure 27. Therefore, before 330 Hz mass transport is complete. This implies that the response time of the device is around 3 ms (=1/330 Hz^{-1}). Current at room humidity (38 % rH) at 1 V is 6.7 μA. Also, when the pressure around the device is decreased from 820 Torrs to ~ 1 Torr, the currents for another 25 μm device increases from ~ 30 nA to 85 nA as shown in Figure 25b. This is expected since the relative humidity goes down with pressure. Such a system therefore could be used as a flow meter where the nanodevice could be placed at two locations, and the pressure drop could be measured.

In summary, an approach is demonstrated for *directed* self-assembly of percolating network of gold nanoparticles on a polyelectrolyte scaffold to produce a highly sensitive and ultra-fast humidity sensor where resistance increases with humidity as against most humidity sensors. The device conductivity changes by 2 orders of magnitude when humidity is brought from 21% to 1.5%. The device's interaction with sound waves showed that the response time of the device is at least 3 ms. showing that the device has one of the best sensitivities with one of the fastest responses. This system could opens up avenues to fabricate systems and devices with complex geometries using polyelectrolyte-formed nano- and micro- structures.

9. CONCLUSION

1. Deposition Mechanism. The high-density deposition mechanism was studied with respect to the super-structure of the bacteria surface, in relationship to the nanometer size scale of the Au particle. The negative charge on the gram-positive bacteria is a result of teichoic acid chains present on the cell wall. Concanavalin A (Con A), interacts specifically with the a-D-glucose-substituted polyglycerol phosphate of teichoic acids on the bacterial surface[75]. Using conjugate of Con A and FITC (photo luminescent dye) the presence of teichoic acid was confirmed. Since teichoic acid is responsible for the high deposition of nanoparticles, capping it affected the deposition of nanoparticles. The high deposition was a result of teichoic acid polyelectrolyte wrapping on the nanoparticle to shield the repulsive force towards other nanoparticles. It was also found using PI/SYTO 9 dye used for 'Live/Dead' test, that the bacteria survive the harsh deposition process and are live for atleast 2 days after deposition.

2. Electron transport mechanism. After conducting experiments at low temperature (4-77 K), the mechanism of electron transfer was found to be electron tunneling with an activation energy of 1.71 and 0.25 meV for bacteria-nanoparticle and PAH-nanoparticle system respectively. Since these are less than kT at room temperature (25 meV), the electron transport in both the cases is through electron tunneling.

3. Bacterial Memory Device. For the first time a new techniques is shown where, image charge attraction is used to change the conductivity of a nanoparticle array. An increase in the conductivity of the bacteria-nanoparticle device is induced by applying a negative potential to one end of the bacteria. This is due to image charge attraction between the nanoparticles in the array and the electrode. This leads to subtle rearrangement of the nanoparticles and formation of new conductive channels. A simple Bethe Lattice model was developed which fit well with the experimental data. The increase in the conductivity was 5 fold for –30V applied voltage.

4. Bacterial Humidity Sensing System. An active hybrid bio-electronic device was built using "physical" nanomaterials and a live microorganism. The bacteria was used as an Nano-electro-mechanical-system (NEMS) where the peptidoglycan layer was actuated using humidity. An < 8% actuation (0.2 nm change in average inter-particle distance) in the peptidoglycan membrane, induced by humidity excursion from 20 to 0%, leads to > 40-fold increase in the tunnelling current. This work is a step forward in providing researchers an avenue to obtain active coupling between microorganisms and (electrical, optical and/or magnetic) physical nanodevices. Such hybrids are the key to conceptually new electronic devices that can be integrated with power and function of microorganisms, on flexible plastic-like substrates using simple beaker chemistry.

5. Nanorods on Bacteria. CTAB, which is an effective surfactant to synthesize variety of shapes of nanoparticles, is used as an effective capping agent for deposition of nanoscale components on the bacteria. The strong electrostatic interaction between

teichoic acid and CTAB coating on nanorods results in bending of the nanorods and a four-order enhancement in conductivity compared to nanospheres. The electrostatic force between the nanorods and bacteria is three orders of magnitude higher than between two self-assembled monolayers of opposite charge. The high conductivity at only ~ 10 % coverage opens the possibility of fabricating electronic circuitry on bacteria without suffocating the microorganism.

6. Nanoparticles on Polyelectrolyte Surfaces. A simple process of directed self-assembly is used to deposit nanoparticles on polyelectrolyte fiber to build world's fastest and most sensitive humidity sensor. In this humidity sensor the resistance increases with humidity (similar to bacterial humidity sensor) as against most humidity sensors. The device conductivity increases by 2 orders of magnitude when humidity is brought from 21% to 1.5%. The device's interaction with sound waves showed that the response time of the device is at 3 ms. This system could opens up avenues to fabricate systems and devices with complex geometries using polyelectrolyte-formed nano- and micro-structures.

10. FUTURE WORK

We have shown that electron tunneling based devices could be built by building percolating array of nanoparticles on oppositely charged polyelectrolyte fingers. Some of the more essential points that we would bring more understanding of the phenomena would be the following: -

1. A study on the mechanism and rate of nanoparticle deposition and change in deposition density with sizes of the polyelectrolyte fingers would give a better understanding of the shielding mechanism of the polyelectrolytes. Based on the angle of wrapping of these polyelectrolyte fingers one could change the shielding strength and hence the distance between the nanoparticles. This required a system with polyelectrolyte fingers having different sizes. This could be achieved by tethering different sized polyelectrolyte by using silane chemistry followed by deposition of nanoparticles. This could also be achieved by using different bacteria with different lengths of teichoic acid. Also, the length of teichoic acid could be controlled on bacteria by changing the amount of phosphorus in the nutrient broth used during the incubation of the bacteria. There isn't much information on the density of teichoic acid on the bacteria. This density would affect the nanoparticle deposition density. A study on this could also be very helpful.

2. Since we already know that percolating array of nanoparticles can be built by using polyelectrolyte we can use this phenomena to build single electron devices. Although each nanoparticle in the array works as a single electron device, the composite-device

does not. But by using a nano-sized fiber we can build a one-dimension electrically percolating necklace of nanoparticles where an electron passing from one electrode to another will pass through all the nanoparticles. This is not the case in a two dimensional array. Having a one-dimensional array greatly increases the coulomb blockade threshold, which could then be used to build non-linear devices. This will also greatly increase the gating operations. In gating a change in potential is produced by an external voltage source, which in turn changes the electronic state of the nanoparticle and therefore changes the coulomb blockade threshold, therefore creating the possibility to build single electron transistors.

3. Single nanoparticle analysis would work as a better system to study the electrical annealing process explained in chapter 4. High resolution SEM could be used to study change in nano displacement of the nanoparticles. This would lead to better characterization of the WORM memory.

4. There could be some modifications made which could produce viable applications.
   a. Since the bacteria is alive for at least one day after the deposition process the physiology of the organism could be used to gate the device. A change in the potential of the bacterial surface occurs because of the ATP cycle of the bacteria.
   b. A conjugate polyelectrolyte-polymer A could be used to build a conjugate fiber. If the polymer A is sensitive to a gas/solvent, then gas/solvent sensors could be built.

REFERENCES

Reference List

1. Su, B., Goldman, V. J. & Cunningham, J. E. Observation of Single-Electron Charging in Double-Barrier Heterostructures. *Science* **255**, 313-315 (1992).

2. Dujardin, E., Peet, C., Stubbs, G., Culver, J. N. & Mann, S. Organization of metallic nanoparticles using tobacco mosaic virus templates. *Nano Letters* **3**, 413-417 (2003).

3. Fowler, C. E., Shenton, W., Stubbs, G. & Mann, S. Tobacco mosaic virus liquid crystals as templates for the interior design of silica mesophases and nanoparticles. *Advanced Materials* **13**, 1266-1269 (2001).

4. Kowshik, M. *et al.* Extracellular synthesis of silver nanoparticles by a silver-tolerant yeast strain MKY3. *Nanotechnology* 95-100 (2003).

5. Li, Z., Chung, S. W., Nam, J. M., Ginger, D. S. & Mirkin, C. A. Living templates for the hierarchical assembly of gold nanoparticles. *Angewandte Chemie-International Edition* **42**, 2306-2309 (2003).

6. Rosi, N. L., Thaxton, C. S. & Mirkin, C. A. Control of nanoparticle assembly by using DNA-modified diatom templates. *Angewandte Chemie-International Edition* **43**, 5500-5503 (2004).

7. Berry, V., Rangaswamy, S. & Saraf, R. F. Highly selective, electrically conductive monolayer of nanoparticles on live bacteria. *Nano Letters* **4**, 939-942 (2004).

8. Chevreau, A., Phillips, B., Higgins, B. G. & Risbud, S. H. Processing and optical properties of spin-coated polystyrene films containing CdS nanoparticles. *Journal of Materials Chemistry* **6**, 1643-1647 (1996).

9. Barry, C. R., Steward, M. G., Lwin, N. Z. & Jacobs, H. O. Printing nanoparticles from the liquid and gas phases using nanoxerography. *Nanotechnology* **14**, 1057-1063 (2003).

10. Hull, P. J., Hutchison, J. L., Salata, O. V. & Dobson, P. J. Synthesis of nanometer-scale silver crystallites via a room-temperature electrostatic spraying process. *Advanced Materials* **9**, 413-& (1997).

11. Paul, S. *et al.* Langmuir-Blodgett film deposition of metallic nanoparticles and their application to electronic memory structures. *Nano Letters* **3**, 533-536 (2003).

12. Decher, G. Fuzzy nanoassemblies: Toward layered polymeric multicomposites. *Science* **277**, 1232-1237 (1997).

13. Schmitt, J. *et al.* Metal nanoparticle/polymer superlattice films: Fabrication and control of layer structure. *Advanced Materials* **9**, 61-& (1997).

14. Trudeau, P. E., Escorcia, A. & Dhirani, A. A. Variable single electron charging energies and percolation effects in molecularly linked nanoparticle films. *Journal of Chemical Physics* **119**, 5267-5273 (2003).

15. Muller, K. H., Wei, G., Raguse, B. & Myers, J. Three-dimensional percolation effect on electrical conductivity in films of metal nanoparticles linked by organic molecules. *Physical Review B* **68**, (2003).

16. Braun, E., Eichen, Y., Sivan, U. & Ben-Yoseph, G. DNA-templated assembly and electrode attachment of a conducting silver wire. *Nature* **391**, 775-778 (1998).

17. Banerjee, I. A., Yu, L. T. & Matsui, H. Cu nanocrystal growth on peptide nanotubes by biomineralization: Size control of Cu nanocrystals by tuning peptide conformation. *Proceedings of the National Academy of Sciences of the United States of America* **100**, 14678-14682 (2003).

18. Shenton, W., Pum, D., Sleytr, U. B. & Mann, S. Synthesis of cadmium sulphide superlattices using self-assembled bacterial S-layers. *Nature* **389**, 585-587 (1997).

19. Flenniken, M. L., Willits, D. A., Brumfield, S., Young, M. J. & Douglas, T. The small heat shock protein cage from Methanococcus jannaschii is a versatile nanoscale platform for genetic and chemical modification. *Nano Letters* **3**, 1573-1576 (2003).

20. Flynn, C. E., Lee, S. W., Peelle, B. R. & Belcher, A. M. Viruses as vehicles for growth, organization and assembly of materials. *Acta Materialia* **51**, 5867-5880 (2003).

21. Trudeau, P. E., Escorcia, A. & Dhirani, A. A. Variable single electron charging energies and percolation effects in molecularly linked nanoparticle films. *Journal of Chemical Physics* **119**, 5267-5273 (2003).

22. Su, B., Goldman, V. J. & Cunningham, J. E. Observation of Single-Electron Charging in Double-Barrier Heterostructures. *Science* **255**, 313-315 (1992).

23. Crommie, M. F., Lutz, C. P. & Eigler, D. M. Confinement of Electrons to Quantum Corrals on A Metal-Surface. *Science* **262**, 218-220 (1993).

24. Ohnishi, H., Kondo, Y. & Takayanagi, K. Quantized conductance through individual rows of suspended gold atoms. *Nature* **395**, 780-783 (1998).

25. Andres, R. P. *et al.* Self-assembly of a two-dimensional superlattice of molecularly linked metal clusters. *Science* **273**, 1690-1693 (1996).

26. Imamura, H. *et al.* Coulomb staircase in STM current through granular films. *Physical Review B* **61**, 46-49 (2000).

27. Middleton, A. A. & Wingreen, N. S. Collective Transport in Arrays of Small Metallic Dots. *Physical Review Letters* **71**, 3198-3201 (1993).

28. Trudeau, P. E., Escorcia, A. & Dhirani, A. A. Variable single electron charging energies and percolation effects in molecularly linked nanoparticle films. *Journal of Chemical Physics* **119**, 5267-5273 (2003).

29. Sato, T., Ahmed, H., Brown, D. & Johnson, B. F. G. Single electron transistor using a molecularly linked gold colloidal particle chain. *Journal of Applied Physics* **82**, 696-701 (1997).

30. Thelander, C. *et al.* Gold nanoparticle single-electron transistor with carbon nanotube leads. *Applied Physics Letters* **79**, 2106-2108 (2001).

31. Brust, M., Bethell, D., Schiffrin, D. J. & Kiely, C. J. Novel Gold-Dithiol Nano-Networks with Nonmetallic Electronic-Properties. *Advanced Materials* **7**, 795-& (1995).

32. Rosidian, A., Liu, Y. J. & Claus, R. O. Ionic self-assembly of ultrahard ZrO2/polymer nanocomposite thin films. *Advanced Materials* **10**, 1087-+ (1998).

33. Trudeau, P. E., Escorcia, A. & Dhirani, A. A. Variable single electron charging energies and percolation effects in molecularly linked nanoparticle films. *Journal of Chemical Physics* **119**, 5267-5273 (2003).

34. Le, J. D. *et al.* DNA-templated self-assembly of metallic nanocomponent arrays on a surface. *Nano Letters* **4**, 2343-2347 (2004).

35. Maeda, Y., Tabata, H. & Kawai, T. Two-dimensional assembly of gold nanoparticles with a DNA network template. *Applied Physics Letters* **79**, 1181-1183 (2001).

36. Li, H. Y., Park, S. H., Reif, J. H., LaBean, T. H. & Yan, H. DNA-templated self-assembly of protein and nanoparticle linear arrays. *Journal of the American Chemical Society* **126**, 418-419 (2004).

37. Kumar, A. *et al.* Linear superclusters of colloidal gold particles by electrostatic assembly on DNA templates. *Advanced Materials* **13**, 341-344 (2001).

38. Nakao, H. *et al.* Highly ordered assemblies of Au nanoparticles organized on DNA. *Nano Letters* **3**, 1391-1394 (2003).

39. Warner, M. G. & Hutchison, J. E. Linear assemblies of nanoparticles electrostatically organized on DNA scaffolds. *Nature Materials* **2**, 272-277 (2003).

40. Bergkvist, M., Mark, S. S., Yang, X., Angert, E. R. & Batt, C. A. Bionanofabrication of ordered nanoparticle arrays: Effect of particle properties and adsorption conditions. *Journal of Physical Chemistry B* **108**, 8241-8248 (2004).

41. Patolsky, F., Weizmann, Y., Lioubashevski, O. & Willner, I. Au-nanoparticle nanowires based on DNA and polylysine templates. *Angewandte Chemie-International Edition* **41**, 2323-2327 (2002).

42. Pum, D. & Sleytr, U. B. The application of bacterial S-layers in molecular nanotechnology. *Trends in Biotechnology* **17**, 8-12 (1999).

43. Dieluweit, S., Pum, D. & Sleytr, U. B. Formation of a gold superlattice on an S-layer with square lattice symmetry. *Supramolecular Science* **5**, 15-19 (1998).

44. Berven, C. A. *et al.* Background charge fluctuations and the transport properties of biopolymer-gold nanoparticle complexes. *Journal of Applied Physics* **92**, 4513-4517 (2002).

45. Traversa, E. Ceramic Sensors for Humidity Detection - the State-Of-The-Art and Future-Developments. *Sensors and Actuators B-Chemical* **23**, 135-156 (1995).

46. S.O.Kasap *Principals of Electrical Engineering materials and devices*. McGraw-Hill, New York (1997).

47. Krasteva, N. *et al.* Self-assembled gold nanoparticle/dendrimer composite films for vapor sensing applications. *Nano Letters* **2**, 551-555 (2002).

48. Wohltjen, H. & Snow, A. W. Colloidal metal-insulator-metal ensemble chemiresistor sensor. *Analytical Chemistry* **70**, 2856-2859 (1998).

49. Zamborini, F. P. *et al.* Electron hopping conductivity and vapor sensing properties of flexible network polymer films of metal nanoparticles. *Journal of the American Chemical Society* **124**, 8958-8964 (2002).

50. Kim, S. *et al.* Near-infrared fluorescent type II quantum dots for sentinel lymph node mapping. *Nature Biotechnology* **22**, 93-97 (2004).

51. Mirkin, C. A., Thaxton, C. S. & Rosi, N. L. Nanostructures in biodefense and molecular diagnostics. *Expert Review of Molecular Diagnostics* **4**, 749-751 (2004).

52. Gole, A. & Murphy, C. J. Seed-mediated synthesis of gold nanorods: Role of the size and nature of the seed. *Chemistry of Materials* **16**, 3633-3640 (2004).

53. Murphy, C. J. Nanocubes and nanoboxes. *Science* **298**, 2139-+ (2002).

54. Murphy, C. J. *et al.* Anisotropic metal nanoparticles: Synthesis, assembly, and optical applications. *Journal of Physical Chemistry B* **109**, 13857-13870 (2005).

55. Sau, T. K. & Murphy, C. J. Room temperature, high-yield synthesis of multiple shapes of gold nanoparticles in aqueous solution. *Journal of the American Chemical Society* **126**, 8648-8649 (2004).

56. Gole, A., Orendorff, C. J. & Murphy, C. J. Immobilization of gold nanorods onto acid-terminated self-assembled monolayers via electrostatic interactions. *Langmuir* **20**, 7117-7122 (2004).

57. Zallen, R. *The physics of amorphous solids*. Wiley, New York (1983).

58. Berry, V. & Saraf, R. F. Self-assembly of nanoparticles on live bacterium: An avenue to fabricate electronic devices. *Angewandte Chemie-International Edition* **44**, 6668-6673 (2005).

59. Connor, E. E., Mwamuka, J., Gole, A., Murphy, C. J. & Wyatt, M. D. Gold nanoparticles are taken up by human cells but do not cause acute cytotoxicity. *Small* **1**, 325-327 (2005).

60. Wu, B., Heidelberg, A. & Boland, J. J. Mechanical properties of ultrahigh-strength gold nanowires. *Nature Materials* **4**, 525-529 (2005).

61. Pasche, S., Textor, M., Meagher, L., Spencer, N. D. & Griesser, H. J. Relationship between interfacial forces measured by colloid-probe atomic force microscopy and protein resistance of poly(ethylene glycol)-grafted poly(L-lysine) adlayers on niobia surfaces. *Langmuir* **21**, 6508-6520 (2005).

62. Pasche, S., Textor, M., Meagher, L., Spencer, N. D. & Griesser, H. J. Relationship between interfacial forces measured by colloid-probe atomic force microscopy and protein resistance of poly(ethylene glycol)-grafted poly(L-lysine) adlayers on niobia surfaces. *Langmuir* **21**, 6508-6520 (2005).

63. Fizazi, A. *et al.* Percolation on A Self-Assembled Network - Decoration of Polyethylene Gels with Conducting Polymer. *Physical Review Letters* **64**, 2180-2183 (1990).

64. Suzuki, Y. Y., Heeger, A. J. & Pincus, P. Percolation of Conducting Polymers on A Gel. *Macromolecules* **23**, 4730 (1990).

65. Gole, A. & Murphy, C. J. Seed-mediated synthesis of gold nanorods: Role of the size and nature of the seed. *Chemistry of Materials* **16**, 3633-3640 (2004).

66. Gole, A. & Murphy, C. J. Seed-mediated synthesis of gold nanorods: Role of the size and nature of the seed. *Chemistry of Materials* **16**, 3633-3640 (2004).

67. Gole, A. & Murphy, C. J. Seed-mediated synthesis of gold nanorods: Role of the size and nature of the seed. *Chemistry of Materials* **16**, 3633-3640 (2004).

68. Gole, A. & Murphy, C. J. Seed-mediated synthesis of gold nanorods: Role of the size and nature of the seed. *Chemistry of Materials* **16**, 3633-3640 (2004).

69. Sau, T. K. & Murphy, C. J. Self-assembly patterns formed upon solvent evaporation of aqueous cetyltrimethylammonium bromide-coated gold nanoparticles of various shapes. *Langmuir* **21**, 2923-2929 (2005).

70. Chen, J., Reed, M. A., Rawlett, A. M. & Tour, J. M. Large on-off ratios and negative differential resistance in a molecular electronic device. *Science* **286**, 1550-1552 (1999).

71. Donhauser, Z. J. *et al.* Conductance switching in single molecules through conformational changes. *Science* **292**, 2303-2307 (2001).

72. Aviram, A. & Ratner, M. A. Molecular Rectifiers. *Chem. Phys. Lett.* **29**, 277 (1974).

73. van Delden, R. A. *et al.* Unidirectional molecular motor on a gold surface. *Nature* **437**, 1337-1340 (2005).

74. Anelli, P. L., Spencer, N. & Stoddart, J. F. A Molecular Shuttle. *Journal of the American Chemical Society* **113**, 5131-5133 (1991).

75. Doyle, R. J., McDannel, M. L., Helman, J. R. & Streips, U. N. Distribution of teichoic acid in the cell wall of Bacillus subtilis. *J Bacteriol* **122**, 152-8 (1975).

76. Kleinsmith, L. J. & Kish, V. M. *Principles of cell and molecular biology*. HarperCollins, New York (1995).

77. Collier, C. P., Saykally, R. J., Shiang, J. J., Henrichs, S. E. & Heath, J. R. Reversible tuning of silver quantum dot monolayers through the metal-insulator transition. *Science* **277**, 1978-1981 (1997).

78. Remacle, F. & Levine, R. D. Quantum dots as chemical building blocks: Elementary theoretical considerations. *Chemphyschem* **2**, 20-36 (2001).

79. Giaever, I. & Zeller, H. R. Superconductivity of Small Tin Particles Measured by Tunneling. *Physical Review Letters* **20**, 1504 (1968).

80. Gorter, C. J. A possible explanation of the increase of the electrical resistance of thin metal films at low temperatures and small field strengths. *Physica* **17**, 777 (1951).

81. Lambe, J. & Jaklevic, R. C. Charge-Quantization Studies Using a Tunnel Capacitor. *Physical Review Letters* **22**, 1371 (1969).

82. Birk, H., Dejong, M. J. M. & Schonenberger, C. Shot-Noise Suppression in the Single-Electron Tunneling Regime. *Physical Review Letters* **75**, 1610-1613 (1995).

83. Andres, R. P. *et al.* Room temperature Coulomb blockade and Coulomb staircase from self-assembled nanostructures. *Journal of Vacuum Science & Technology a-Vacuum Surfaces and Films* **14**, 1178-1183 (1996).

84. Heath, J. R., Knobler, C. M. & Leff, D. V. Pressure/temperature phase diagrams and superlattices of organically functionalized metal nanocrystal monolayers: The influence of particle size, size distribution, and surface passivant. *Journal of Physical Chemistry B* **101**, 189-197 (1997).

SUPPLEMENTARY BACKGROUND INFORMATION

1. MATERIAL USED

BACILLUS CEREUS

Bacillus cereus is a gram-positive rod-shaped bacterium. It is around 4-5 microns long and about 1 micron wide. It grows on nutrient media at 30.5 ^{o}C with log-phase of growth at around 14 hrs.
As most gram-positive bacteria, this bacterium also has negatively charged teichoic acid on its surface.
This is a very benign bacterium, which is ready found in rice and other foods. Upon a lot of intake, these bacteria can cause food poisoning and diarrhea.

GOLD NANOPARTICLES

The gold nanoparticles used in this study are 30 nm in size. They are negatively charged because of the Cl_4^- group attached at the surface of the nanoparticles. The particle density is 2 X 10^{11} particles per ml. The absorption peak for these particles is at around 525 nm.

POLY-L-LYSINE

Poly-L-Lysine is a protein polyelectrolyte. The structure of lysine used in this study is given below.

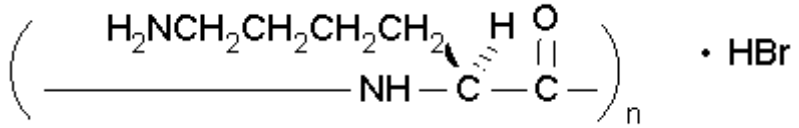

It is a hydrobromide salt and comes in various degrees of polymerization (DP). The ones used in this study are DP – 4, 10, and 1500.
Poly-L-Lysine when dissolved in water gets positively charged because of protonation of the amine group by the following reaction: -

$R\text{-}NH_2 + H^+ \rightarrow R\text{-}NH_3^+$

This positively charged polyelectrolyte would deposit readily as a monolayer on a negatively charged surfaces. As most proteins, poly-L-Lysine shows an absorption peak at around 230 nm.

2. COMMON TERMINOLOGIES

EXTRA-CELLULAR POLYMERIC SUBSTANCES (EPS)

EPS are biopolymers excreted by bacteria. These generally compose of polysaccharides, and proteins. Most of these are excreted as a defense mechanism against threats like toxins and endotoxins.

3. EXPERIMENTAL TECHNIQUES USED FOR THIS STUDY

3.1 INTRODUCING NEGATIVE CHARGE ON SILICA

Negative charge on silica surface was introduced by oxygen plasma treatment on the silica surface. The plasma of pressure 600-700 mTorr and power 100 Watts was exposed on the silica surface for 120 seconds. This led to generation of SiOH groups on the silica surface. The oxygen plasma creates highly reactive sites on silica, which then picks up moisture from the air and creates SiOH groups on the surface. When this plasma treated silica is put in water it generates negative charge by the following reaction: -
$SiOH \leftrightarrow SiO^- + H^+$
The oxygen plasma cleans the surface of most organic deposits. Since the plasma etches silica, the time of etching has to be optimized.

Plasma treatment can be tested by a simple wetting experiment. The surface becomes highly hydrophilic after the plasma treatment. Also the plasma treatment has to be done very cleanly. Other gases might be present in the plasma system that can create some other groups on the silica. The plasma can be checked by looking at its color. For oxygen plasma the color should be white/blue. If the color is pink then it indicates nitrogen contamination in the plasma.

4. BACTERIAL SURFACE PROPERTIES

4.1 Cell Wall of bacteria

The surface of bacteria is very complex as compared to animal or plant cell. The bacterial cell is enclosed by several discrete structures collectively known as cell envelope[76]. This envelope consists of the plasma membrane and a relatively rigid cell wall. This wall is strong and protects the cell from physical and chemical attacks. For example a large number of bacteria is found in waters with a low concentration of salt. This leads to osmosis into the bacteria leading to a high pressure inside the bacteria, which can burst the cell, if the cell wall is weak. But the strength of the cell wall protects the bacteria from bursting.
Bacteria come in various shapes, but the most common ones are bacilli (rod shaped), cocci (spherical shaped) and spirilla (spirally shaped). Based on the reaction to a staining procedure the bacteria are classified into two categories. In this procedure, the bacterial cell wall is stained with a basic dye usually crystal blue and then is washed using an alcohol. The bacteria that retain the stain after the alcohol wash are referred to as gram-positive and the ones that do not retain the stain are referred to as gram-negative bacteria. This difference in staining response reflects a difference in cell envelope organization for gram-positive and gram-negative bacteria, which is discussed below.

a. Gram-positive

Gram-positive bacteria have thick cell wall located immediately outside the plasma membrane. This cell wall mostly comprises of a polysaccharide-peptide complex known as murein or peptidoglycan. The diagram below shows the cell wall organization for gram-positive bacteria.

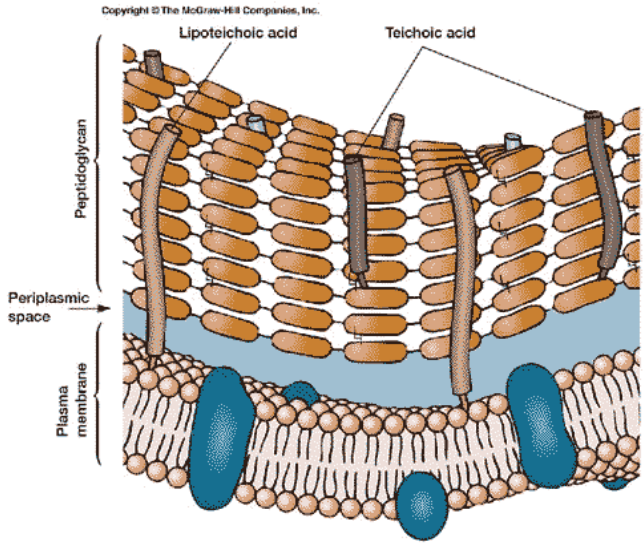

Schematic of the cell wall of Gram-positive bacterium. It can be seen that the teichoic acid and polytechoic acid is exposed to the outside of the cell wall.

The polysaccharide portion of peptidoglycan consists of alternating residues of N-acetylglucosamine and N-acetylmuramic acid. N-acetylmuramic acid is a lactic acid derivative of glucosamine. These polysaccharides have peptide bridges connecting N-acetylmuramic acid groups of adjacent chains to each other. These peptide bridges are generally made of only a few kind of amino acids like D-amino acids and some unusual amino acids like diaminopimelic acid (close relative to lysine). The diagram below shows the peptide bridges holding the peptidoglycan.

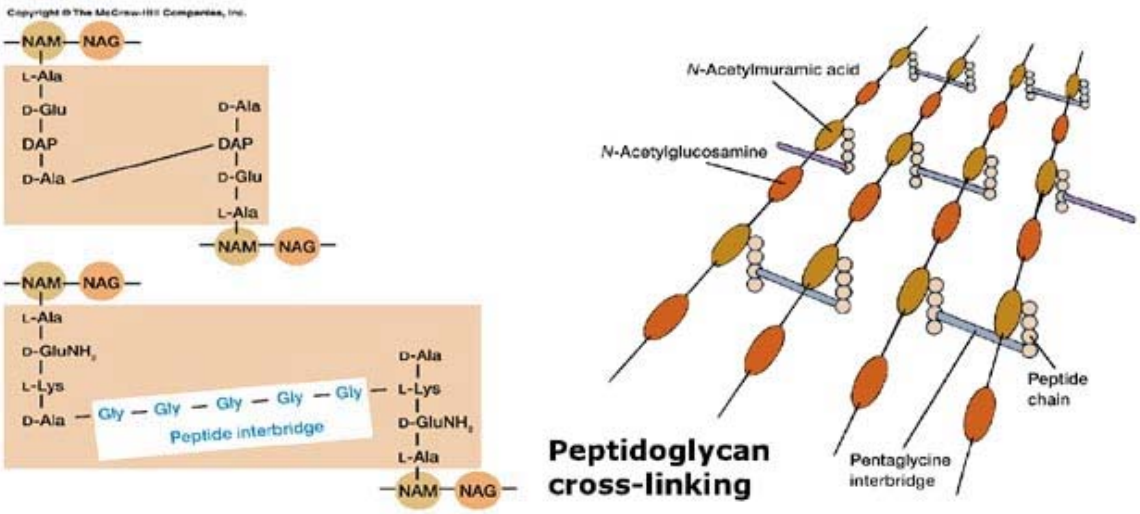

Schematic showing the cross-linking in the peptidoglycan layer, which provides strength to the structure and extra protection to the cell membrane.

This cross-linking of the polysaccharide chains by peptide bridges forms an intertwined network imparting great strength to the cell wall.
Evidence of peptidoglycan was found from a study involving lysozymes. Lysozymes are enzymes that hydrolyze the polysaccharide chains of peptidoglycan. Gram-positive bacteria treated with lysozymes lose their cell wall creating wall-less cell called protoplasm, which are spherical is shape irrespective of the original shape of the bacteria.
Also interwoven into the peptidoglycan framework are special molecules, most prominent of which is teichoic acid. We will discuss about teichoic acid in detail later in this section.

b. Gram-negative
In gram-negative bacteria the cell wall the peptidoglycan layer is thinner than that in gram-positive bacteria. This makes the cell wall weaker than gram-positive cell wall. Also since the peptidoglycan layer is thin the gram staining dye is easily dissolved in the alcohol wash. Gram-negative cell wall also consists of an outer membrane (lipid bilayer) external to the peptidoglycan layer. The inner leaflet of this bilayer consists of membrane phospholids, while the outer leaflet contains lipopolysaccharides rather than phospholipids. Lipopolysaccharides are complex chains of sugar molecules with fatty acid residues covalently attached at one end. While the polysaccharide end is hydrophilic because of the presence of sugar molecules, the fatty end is hydrophobic making the lipopolysaccharide amphiphatic. Therefore the fatty acid hydrophobic end is buried in the membrane interior and the hydrophilic sugar chains are exposed to the outer membrane surface. The diagram below shows the cell wall organization of a gram-negative bacteria

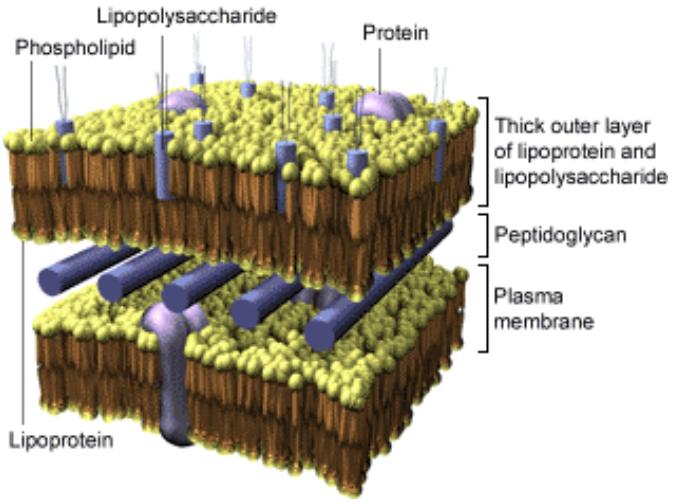

Schematic of the cell wall of Gram-negative bacterium. It can be seen that the peptidoglycan layer is not the outer most layer of the cell wall.

The outer membrane of the gram-negative bacteria also contains several dozens of proteins. The functions of these proteins have been investigated by studying the properties of mutant strains of bacteria in which one protein is either missing or defective. Such studies have shown that while some proteins are just structural proteins helping maintain membrane integrity, other proteins may function as cell surface receptors, anchoring sites for external structure or transporters for uptake and export of specific molecules. Especially important in this regard are proteins called porins, which function as hydrophilic membrane pores for passive diffusion of water-soluble molecules.

4.2 Teichoic acid

Teichoic acids are linear polymers of glycerophosphate or ribitolphosphate carrying sugar or D-alanine substitutes, present in the peptidoglycan layer of gram-positive bacteria. Their chain length varies from 8 – 50 units.

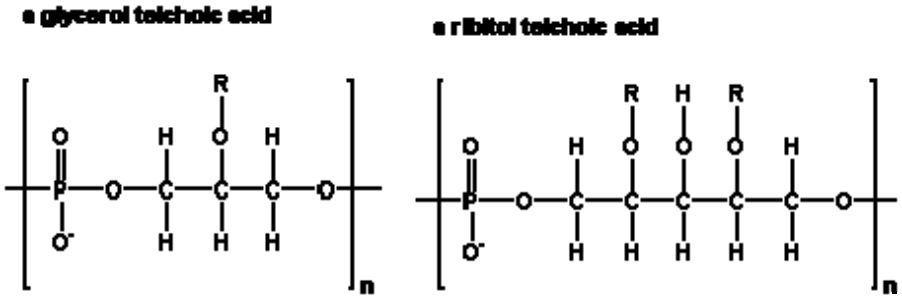

Chemical formula of teichoic acid showing that the polymer is anionic.

It is clear from the structure above that these are anionic bio-polymers. They are known be antigenic.
Experiments have shown that the teichoic acid is present only in the exterior of the gram-positive bacterial cell walls. 50% of teichoic acid is in the peptidoglycan layer while the other 50% is present on the surface of the bacteria. This was found by an experiment done by Doyle et al[75]. The group used Concanavalin A (Con A) as a teichoic acid receptor during autolysis of bacillus subtilis cell wall. In the study it was found that 50% of the total Con A precipitation was at the early stage of autolysis of the bacterial cell wall. The remaining Con A was precipitated regularly as the bacterial cell wall underwent autolysis. This suggested that half of teichoic acid in the cell wall is on the exterior of the cell wall, while the other half is distributed evenly in the peptidoglycan layer. When a fluorescent labeled Con A was used on the bacterial cell walls it was found that the cell wall was completely covered with teichoic acid.

5 ELECTRICAL PROPERTIES OF METALLIC NANOPARTICLES

Electronic model

The electronic Hamiltonian used to describe a metal nanoparticle regards each as having one valence electron. This electron is confined to the metal nanoparticle and therefore its energy scales to the size of the particle, as is the case for a particle in square well potential. The other electrons of the nanoparticles are in the core and are assumed to be frozen. When two metal nanoparticles come sufficiently close to each other their valence orbitals overlap. This allows the electron to tunnel through one nanoparticle to another and couple them. In the case of a closely packed nanoparticle array, the electronic state is fully delocalized. When the array is expanded to let the distance between the nanoparticles increase there is a delocalized-to-localized transition, because as the strength of the transfer integral decreases the disorder and the coulombic effects begin to dominate.

Apart from the coulombic effects, described latter, the other factor that affect the electronic properties of an array of nanoparticles is disorder. In a nanoparticle array, the kinds of disorders that influence the electronic properties are size fluctuations and lattice compression.

The fundamental difference between a nanoparticle array and a solid is the size fluctuation. Each lattice site in a solid is identical, but in the case of nanoparticle prepared by the techniques explained earlier, even though the shape is approximately the same, there is difference in the size of the nanoparticle. This affects the electronic properties like ionization potential and charging energies (explained below), which are size dependent. The other disorder for most of the self-assembled monolayers (SAMs) of metal nanoparticles on various substrates is – no definite lattice structure. In most cases the SAMs are random arrays of nanoparticles. The conduction through these arrays is possible only if the nanoparticle density is above the percolation threshold. Also the thermal motion of the particles can cause a change in the inter-particle distance.

If the metal-nanoparticle-arrays are not formed by SAM, but by langmuir technique, then there is a larger control over the lattice geometry and lattice compression[77]. Nanoparticle separation can also be tuned by varying the length and nature of the ligand used to passivate the nanoparticle. Other method to control the distance is by using electric and/or magnetic field. If D is the center-to-center distance between the nanoparticles of radius R, then, it has been found that an array with $D/2R > 1.8$ is not conducting. Various studies have shown varying results for $1.2 > D/2R > 1.8$. For $D/2R < 1.2$, the array has been found to have ohmic behavior[78].

Electronic properties of metallic nanoparticles

The electronic properties of a metallic nanoparticle array surrounded by insulator (media) are governed by three parameters. These are

1. the charging energy of the nanoparticle,
2. the inter-particle distance and
3. the orientation of a nanoparticle with respect to its neighbor and the arrangement of the nanoparticle array.

The electronic properties of nanoparticle-array are somewhere between that of bulk state and molecular state. For a molecule, the energy needed to add an electron and remove an electron are different and are called the electron affinity and the ionization potential. For the bulk these two energies are equal to the work function of the metal. In the case of a metallic nanoparticle these two energies are close to the work function but not equal. Both the ionization energy and the electron affinity approach work function as the size of the particle increases. The ionization energy approaches the work function from the top while the electron affinity approaches it from bottom. The charging energy is the difference between electron affinity and ionization potential for the particle. The charging energy ε_c is given by $\varepsilon_c = \frac{e^2}{C}$, where e is the fundamental unit of charge and C is the capacitance of the nanoparticle. The capacitance of the nanoparticle is dependent on the size of the particle, $C(r) = 4\pi\varepsilon_o \varepsilon r$, where ε is the dielectric constant of the media around the nanoparticle and r is the radius of the nanoparticle. The charging of the nanoparticle can happen only in multiples of electron charge. If the capacitance is reduced, the charging energy will increase, and can eventually exceed the thermal energy. At this point, the charge quantization

effects of charging nanoparticles can be observed. The charging energy can thus block the entrance of additional electron to the nanoparticle. This phenomenon is known as Coulomb blockade.

To observe coulomb blockade, the metal nanoparticle should be separated by a very thin insulating layer on both sides and the wave-function of the electron on both sides of the nanoparticle should overlap so that there is a finite probability of the electron tunneling through the junction. The capacitance of the junction would then be around 10^{-15} to 10^{-16} F and the corresponding charging energy would be 1 to 10K. Since coulomb blockade can be observed only in processes where there is electron transfer taking place through a metal island (nanoparticle), the nanoparticle has to be connected to the electrical field without the electric field having any effect on the capacitance and thereby changing the charging energy. When such a system is built, it is seen that after a certain threshold voltage, the electron tunnels with a rate proportional to $V/(eR_T)$, where R_T is the tunnel resistance. Therefore, the charge can be added and removed from the nanoparticle in discrete units through the tunneling process. Also essential for this is that the charge be localized on either side of the nanoparticle. For this, thermal and quantum fluctuations of the electron must be minimum.

$E_C >> E_T$

Perturbation calculations have shown that the quantum fluctuations are negligible.

Or, $R_T >> R_K$

Where R_K is the quantum resistance ($= h/e^2 = 25.8\ K\Omega$)[79-81].

Another capacitor can now be added to the system to couple with the metal nanoparticle. This capacitor can be connected to a power source and can be used to induce polarization on the metal nanoparticle and thus control its potential. This capacitor is called the gate capacitor. By changing the voltage attached to this capacitor the potential on the nanoparticle can be tuned to control the flow of electron through the nanoparticle. This device is called a Single Electron Transistor (SET)[82]. A diagram to explain this process is shown below.

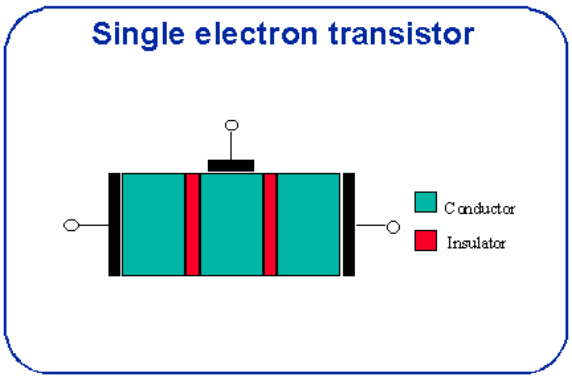

Schematic showing a single electron transistor in which the potential on a nanoparticle is controlled by an attached gating electrode.

Andres and group[83] used the aerosol technique to prepare thiol passivated gold nanoparticle monolayer on a conducting substrate. An STM was used to measure the electrical property of these nanoparticles. The STM tip was used as an electrode and the electron transfer was studied from single nanoparticle to the STM tip. The capacitance was so small that Coulomb blockade and Coulomb staircase effect were observed at room temperature. Heath and coworkers also built a similar capacitive device by putting a monolayer of silver nanoparticle on the surface of a conducting substrate by Langmuir technique and then spin-coating a thin polymer layer on top of it. On this polymer layer they put another conducting layer. These two conducting layers were the electrodes across which capacitance was measured with respect to the applied voltage. In this case nanoparticles were in parallel to each other and therefore the electrical properties measured were magnified version of those between two nanoparticles and not across the nanoparticle array[84]. They also observed Coulomb blockade at room temperature.

VITA

Vikas Berry received his Masters of Science in Chemical Engineering from University of Kansas and Bachelors of Technology in Chemical Engineering from Indian Institute of Technology, Delhi. As a Research Assistant, while completing his Doctorate of Philosophy from Virginia Polytechnic Institute and State University, he conducted research in the area of Bionanotechnology. He also worked as a Research Executive in Cadila Pharmaceuticals in India.

He is married to Namrita Vikas Berry and is son to Lt. Col. V. K. Berry and Raj Berry. He was born on 9th August 1977 in the city of Pune in India.